A Simplified Approach to Estimate the Area of Interest Coverage Duration Performance for SAR Satellites

Allan Bojarski, Markus Bachmann

German Aerospace Center (DLR), Microwave and Radar Institute, 82234 Wessling, Germany
allan.bojarski@dlr.de

***Abstract*—During the mission design for Synthetic Aperture Radar (SAR) Earth observation satellites, the coverage capabilities are a key parameter for the performance of the system. In addition, they have a direct influence on the further mission concept and the design of an observation scenario. A representative coverage analysis regarding the time to cover relevant targets must be conducted by evaluating the coverage durations for various dimensions of areas of interest (AOIs) in multiple globally distributed locations. For this purpose, common approaches generally achieve comprehensive and precise results but also require cumbersome software configurations to realize a wide variety of scenarios adopting various AOI dimensions and locations. In this paper we therefore introduce a dedicated and simplified approach to estimate the coverage duration performance of a SAR system which can be achieved with few input parameters for various AOIs thus providing an advantage in early stages of the mission design. In this context the presented coverage estimations are performed using basic orbit characteristics, including for example the number of days per repeat cycle or the orbit's inclination and the effective swath width of the SAR system. By evaluating the geometric relations between the AOI and the swath as well as by determining the revisit and access possibilities from the repeat ground-track orbits, the coverage duration is approximated for each AOI dimension. With this methodology the coverage durations for various orbital configurations and swath widths can be analyzed and compared against each other effectively. The results then provide an overview of the coverage duration performance of different configurations and can either be used to derive necessary improvements or to evaluate the current configuration.**

***Index Terms*— Synthetic Aperture Radar, Planning, Approximation methods**

I. Overview

A. Introduction

During the initial design phases of Synthetic Aperture Radar (SAR) missions, the imperative performance criteria for accomplishing mission goals are established. These criteria subsequently guide the iterative process of payload system design or vice versa. A key performance metric among these is the system's coverage capability which depends on both the SAR system performance as well as the orbit characteristics. In general, it can be stated that the faster mission relevant areas are acquired, the more data can be captured in shorter time periods. This again leads to a faster achievement of the mission objectives or provides the opportunity for an optimized acquisition strategy. Thus, the assessment of a system's capability to achieve a fast coverage of relevant targets stands as a pivotal performance benchmark making its evaluation essential in particular in early stages of the mission design.

In general, a complete coverage duration analysis of a system must be conducted by computing the durations to cover various areas of interest (AOIs) in various, globally distributed locations. In this context coverage duration refers to the time between the first and the last acquisition which are required to completely cover the AOI. Common techniques therefore often employ numeric methods such as the grid-point approach as discussed in detail in [1] - [4]. The approach is applied by generating graphical propagation scenarios using uniformly sampled grid points in combination with the brute force method to determine the access possibilities to the AOI [5]. The achievable coverage and the according coverage duration for any AOI is then determined by simulating the orbit of a spacecraft and evaluating the intersections of the system's footprint, i.e. the swath, with the grid points of the AOI location over the desired simulation time. Prominent software that uses the grid-point approach are for example the Systems Toolkit (STK) [6] and the FreeFlyer Astrodynamics Software [7]. On the one hand, this methodology achieves very precise and comprehensive coverage results which allow a detailed analysis of the coverage performance. The coverage duration for example is generally determined with millisecond accuracy. For simple coverage scenarios with few configuration changes and few AOIs to be analyzed, the according numeric software solutions are therefore the preferable choice. On the other hand, analyzing a multitude of different orbit and sensor configurations as well as various AOIs requires considerable effort. In particular, software tools that use a graphical scenario configuration (e.g. STK and Freeflyer), become quickly complex for increasing number of configurations and AOIs. As they usually generate individual scenarios for each system configuration, simulating multiple variations of configurations is difficult to navigate. Furthermore, an evaluation of the coverage duration from these simulations requires a further

external processing due to the extent of the results. STK for example generates text files for each configuration containing each access to each of the specified AOIs. Without external processing it is then difficult to derive an overview of the coverage duration.

Besides the pure numeric methods, there are also analytic approaches to determine the coverage duration of an AOI. Examples are 2D mapping [8], the route theory for constellations or geometric analysis such as field mapping [9] or polygon clipping [10]. However, all of them rely on the grid-method to generate the coverage performance for a given target as explained in [11] and are therefore regarded as hybrid solutions. Although all of them require significantly less computational effort and some can handle multiple variations of the input parameters, they experience various drawbacks. Some of them provide only a limited coverage characteristic because the field of view or the repeat cycle is static as for example in 2D mapping, while some are merely suitable for the coverage analysis of single satellites as for example the field-mapping approach. Furthermore, none of them is designed to compute coverages performed by a SAR system using rectangular swaths and considering multiple beams.

In summary, the advantage of the grid-point approach, hybrid solutions and other related methods such as point groups [7] or more complex approaches, based for example on polygons as described in [12] - [15], is that they provide a precise solution to determine the coverage performance in terms of coverage duration, revisit time and percent coverage in certain time intervals among others. However, by developing a dedicated method to explicitly determine the coverage duration, the effort can be significantly reduced and generating a representative overview over various AOI ranges becomes less complex.

Therefore, this paper introduces an approach to estimate the coverage duration for a SAR system based solely on the required parameters. SAR system specifics are introduced by addressing side-looking acquisitions (e.g. because of the usually right-looking antenna) and constraints regarding different SAR applications such as interferometry or applications that require a stable backscatter. The relevant parameters to estimate the coverage duration include the orbit characteristics in terms of number of days per repeat cycle (RC), number of orbits completed per repeat cycle R and the inclination of the orbit as well as the effective swath width of the system. The orbit parameters can be chosen from basic orbit geometry considerations for repeat ground-track orbits as described in [16], [17] and [18] while the swath width is obtained from the mission requirements in a trade-off between the SAR performance parameters [19]. The number of necessary acquisitions for each AOI is then derived by evaluating the geometric relations between the swath width and the AOI extent in latitude and longitude. Considering the influence of the overlapping access ranges (ARs) towards the poles and the time to reach the according orbits that have an access to the AOI, the final coverage duration for an AOI in the order of days is estimated. The examples to demonstrate the methodologies presented in the following, are based on the TerraSAR-X satellite and its orbit characteristics. Flying in a close formation with its twin, the TanDEM-X satellite, in nearly the same orbit, the almost identical remote sensing satellites are designed to acquire monostatic and bistatic SAR images of the Earth [20].

The proposed solution provides a dedicated approach to analyze the coverage duration for various orbit and system parameters as well as different AOI dimensions and locations. Although the results do not achieve the same level of precision as conventional methods, they rely on only a few fundamental parameters providing a simplified and suitable assessment of the coverage duration of the analyzed configuration. The suggested approach is an extension to the methodology presented in [21] by further discussing the details of achieving coverage of an AOI and above all including the combined use of ascending and descending beams in the coverage duration approximation.

Figure 1 illustrates a schematic coverage of an AOI as it would be performed by a right-looking SAR satellite traveling in an ascending orbit from south to north. The figure shows the key parameters that are required to compute the coverage duration. The upcoming sections are dedicated to the determination of these parameters and the paper is therefore structured as follows. Chapter II explains how to determine the number of acquisitions defined as n_{acq} which are needed to entirely cover the AOI based on the exclusive or combined use of ascending and descending acquisitions. Chapter III elaborates on the approach to compute the accessibility of an AOI from multiple orbits being represented by the maximum number of orbits with an access to the AOI, defined as n_o. The section is followed by the derivation of the coverage duration t_{cov} in the order of days, based on n_{acq}, n_o and the time to reach the adjacent orbits, in chapter IV. The chapter also provides coverage estimation results considering various coverage scenarios as well as a comparison with real mission planning data. The paper is then finalized by summarizing the presented approach in chapter V and giving a conclusion based on various simulations and validation results in chapter VI.

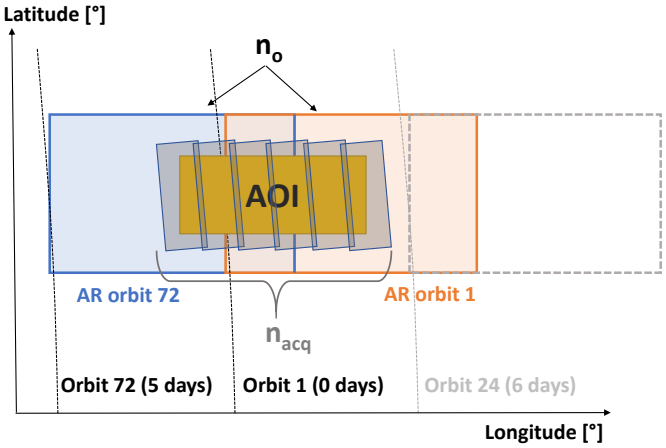

Figure 1: Schematic AOI coverage by a SAR satellite from an ascending orbit with six right-looking acquisitions, illustrating the key parameters (n_{acq}= 6, n_o = 2 and days to reach the orbits (5 days for orbit 72 or 0 days for orbit 1)) to approximate the coverage duration by means of the presented approach.

B. Assumptions

As addressed in the introduction, the presented methodology performs an estimation of the duration, in the amount of days, that are required to completely cover an AOI. This estimation is based on a simplified geometric analysis of the intersections of the swath and the AOI. The presented approach is therefore subject to various assumptions that enable a simplification of performing a coverage estimation for a given AOI. They are summarized and listed in the following:

- Flat Earth: the approach assumes a flat Earth geometry which enables the use of rectangular instead of trapezoid shaped AOIs with curved sides when using a two-dimensional representation of a spherical surface. This simplifies the geometric analysis by avoiding the application of spherical geometry for the intersection of the footprint and the AOI on ground. In order to give an estimate of the error introduced by this assumption, we analyze the difference in projection width (longitude direction) and height (latitude direction) from a spherical to a flat surface. We therefore exemplarily define a reference scenario with a desired projection width of 100 km in longitude and 40 km in latitude at the equator. This reference scenario is later also used to present the results of the described approach (e.g. in **Figure 22**). In height the projection difference is negligible due to the small change in latitude and the large radius of the Earth. For a 40 km distance in latitude the difference for a flat surface projection is less than 10 cm. At larger height distances of up to 1000 km, the difference is still less than 1 km, i.e. less than 0.1%. To estimate the error in longitude direction we use Tissot's indicatrix and compute the difference in projection width between two different latitudes for a projection onto a flat surface [22]. Using again the reference scenario, the difference in the projection width between latitudes of for example 48° and 48.4° (equal to 40 km distance in latitude direction), results in 0.5 km. This difference increases, when the projection is performed closer towards the poles. At 71° and 71.4° for example, the difference is at 0.7 km. Both examples are still much less than the typical overlap between the swaths of the single beams. Nevertheless, in order to compensate this introduced error, we analyze the coverage duration for a best and worst case regarding the access to an AOI. Further details are presented in section II.B and section III.C. The final coverage duration results then represent an approximation and are presented accordingly in section IV. Another consequence of the flat Earth assumption is that further Earth curvature effects are not considered which for SAR systems in particular relates to the increasing swath width between near- and far-range footprints. In order to overcome this issue for sensors that keep a constant incidence angle range for each beam, the swath width is approximated by defining an average swath width. This may lead to slight uncertainties in the geometric analysis but is also compensated for by performing the above described best- and worst-case analysis for each coverage. However, SAR systems generally adjust the incidence angle range of each beam to keep the swath width constant from near to far range. In these cases, the average swath width represents the actual swath width of the system.
- Shape and orientation of an AOI: in the analysis of the intersections with an AOI, the AOI is defined to be of rectangular shape. Including arbitrary AOI shapes would significantly increase the complexity or even hinder the feasibility of the approach. Furthermore, an AOI is defined to be always horizontally oriented in longitude direction and vertically oriented in latitude direction.
- Beam inclination: for the sake of simplification, the beams of the SAR antenna shall have the same inclination as the orbit. This means also that the beams from adjacent orbits are assumed to be parallel for all latitudes and that their pointing direction is parallel to the longitude direction. As a result, the beams of adjacent orbits do not change their orientation to one another over the orbit. This is true at the equator and negligible in its near vicinity (±20°) as the effects are small (< 1° for TerraSAR-X orbit) and are compensated by the overlap between the beams. With increasing latitudes however, the beam inclination and the alignment between the beams from adjacent orbits significantly changes due to the ground-track projection on a two-dimensional surface and to the rotation of the Earth. In order to compensate this effect, latitude- and AOI size-based margins are included. Further details on the derivation and application of those margins are given in section III.E.
- Instantaneous beam coverage: since the duration of the beams' access to an AOI during each pass is not determined in the presented approach, the coverage of each beam over an AOI is assumed to be instantaneous. As a consequence, the rotation of the Earth during the pass and in particular the drift of the ground-track in this time is not considered. However, the uncertainty introduced by this assumption is rather small and is compensated for by considering a best and worst case as described above in the flat Earth assumption. In order to provide an example of the introduced error, we select the TerraSAR-X satellite which moves with an orbital speed of 7.6 km/s. The rotational speed of the Earth at the equator is approximately 456 m/s, which means that when the satellite covers an AOI with an extent of the before defined reference scenario of 40 km in latitude direction, the AOI will drift 2.4 km westward during the time TerraSAR-X needs to pass the AOI. This drift furthermore becomes smaller towards the poles. At 50° latitude for example, the rotational speed of the Earth reduces to roughly 299 m/s and the AOI drift therefore to 1.6 km.

It is obvious that with the presented assumptions, exact coverage results are not achievable. The approach is therefore presented as an estimation of the coverage duration obtained by analyzing the best and worst coverage possibilities in term of coverage duration. In order to compensate the errors introduced by different approximations, margins are added according to certain conditions. Details on how these margins are derived and applied are given in each of the main sections throughout the paper.

II. Determination of the Number of Necessary Acquisitions for AOI Coverage

The first step to estimate the coverage duration, which is the time in days to completely cover an AOI, is to determine the number of acquisitions that are required for the complete coverage. As this number considerably variates with any data-taking constraints such as the exclusive use of either ascending or descending acquisitions, the following chapter presents solutions for different restrictions including incidence angle accessibility and viewing geometry requirements.

A. *Freely Steerable Beams*

The most optimal AOI coverage is achieved for beams that can be adapted to the targeted area within the accessible range of the antenna, i.e. for beams that are freely steerable. In common SAR systems this is for example implemented for the Spotlight mode which adapts the beams that are required for the coverage to the desired center coordinate as described in [23]. Although the Spotlight mode is generally used to only cover small AOIs (in the order of 10 km x 10 km), the concept of freely steerable beams is indispensable for the basic understanding of the derivation of n_{acq}, and is therefore used in the following as an introduction to the analysis.

The number of required acquisitions for these freely steerable beams is then independent from the location of the AOI within this range. It is only affected by the constraints of the acquisitions, i.e. whether a repeat-pass coverage or a single-pass coverage can be performed. The difference between both lies mainly in the mixed or exclusive usage of ascending and descending orbits. For both cases the relevant parameters are the AOI length in longitude l_{AOI}, the AOI height in latitude h_{AOI} and the delta inclination angle $\Delta i = |i - 90°|$ of the orbit. Furthermore, the effective swath width of the system r_{swath}, i.e. the swath width without considering the swath overlap to the adjacent beam, as for example visible in **Figure 2**, needs to be considered.

a) Single Acquisition Direction Coverage

For most SAR applications, the looking direction cannot be freely changed for the sake of coverage optimization as the applications are sensitive to variations in the viewing geometry. Above all this relates to interferometric applications and in particular to complex image registration as well as to shadow and layover areas in interferometric products as described in [24] and [25]. Also, applications that evaluate parameters depending on the backscatter preferably require similar looking directions as presented in [26].

Since the incidence angle variations in these cases need to be kept at a minimum, an AOI has to be covered from either ascending or descending orbits. **Figure 2** therefore displays a coverage performed exclusively from an ascending direction.

Due to the fixed orientation of the AOI, as mentioned in section I.B, and the inclined orbit, the beams are not parallel or rectangular to the shape of the AOI. As can be seen in **Figure 2** they are angled against the latitude side of the AOI and their effective coverage range in longitude thus differs from the effective swath width. In order to determine the effective

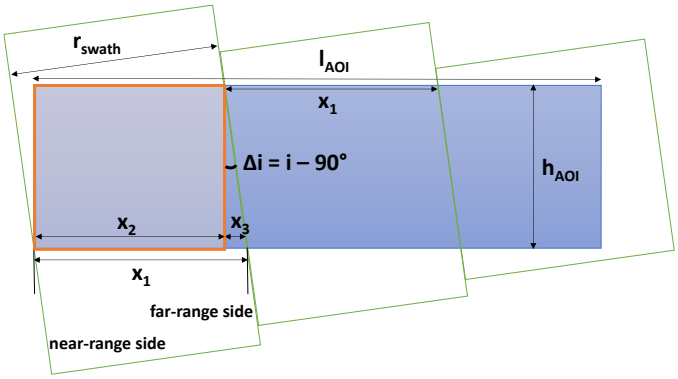

Figure 2: AOI coverage from three right-looking ascending beams and effective coverage parameters $x_1 - x_3$.

coverage of the beams, we therefore define the parameters, x_1, x_2 and x_3, which represent the intersections of one beam with the AOI. Utilizing the effective swath width and the delta inclination angle, these can be derived from the geometric relations as shown in **Figure 2**. The parameter x_1 represents the distance between the near-range and the far-range side of the beam parallel to the longitude direction, x_3 represents the distance in longitude direction between the upper and lower intersection edge of the beam with the AOI and x_2 is defined as the effective coverage distance of the first beam in longitude direction. Mathematically these parameters can be expressed as:

$$x_1 = \frac{r_{\text{swath}}}{\cos \Delta i} \tag{1}$$

$$x_3 = h_{\text{AOI}} \cdot \tan \Delta i \text{ for } h_{\text{AOI}} < \frac{r_{\text{swath}}}{\sin \Delta i} \tag{2}$$

$$x_2 = x_1 - x_3 \tag{3}$$

The expression in (2) shows that at a certain height, x_3 becomes greater than x_1 and thus x_2 becomes negative. Hence the term is only applicable for a limited height of the AOI depending on the effective swath width and the delta inclination angle. For a more general description of x_3 we have to analyze the presented configuration for AOIs beyond this height limit, in particular the geometric relations on the upper edge of these AOIs. **Figure 3** therefore shows a coverage of an AOI with the same length as the one shown in **Figure 2** but larger in height than the height limit h_{lim} specified in (2):

$$h_{\text{lim}} = \frac{r_{\text{swath}}}{\sin \Delta i} \tag{4}$$

It can be seen that the situation described in **Figure 2** begins to repeat at the height at which $h_{\text{AOI}} = h_{\text{lim}}$. This means we can change the expression in (2) to be applicable for all h_{AOI} by using the modulo operator:

$$x_3 = (h_{\text{AOI}} \,\%\, h_{\text{AOI,lim}}) \cdot \tan \Delta i \tag{5}$$

Furthermore, for deriving the number of required acquisitions we then utilize the expressions presented in (1), (3) and (5) and

append additional acquisitions in multiples of h_{lim}. Thus, from the coverage scenario in **Figure 2** and **Figure 3** we derive that the first part of the AOI (red) is effectively covered by x_2 while the remaining part (yellow) is effectively covered by multiples of x_1. By adding multiples of h_{lim} we then obtain the number of required acquisitions $n_{\text{acq,single}}$ using only ascending or descending beams, from:

$$n_{\text{acq,single}} = \left\lceil \frac{l_{\text{AOI}} - x_2}{x_1} + \left\lceil \frac{h_{\text{AOI}}}{h_{\text{lim}}} \right\rceil \right\rceil \qquad (6)$$

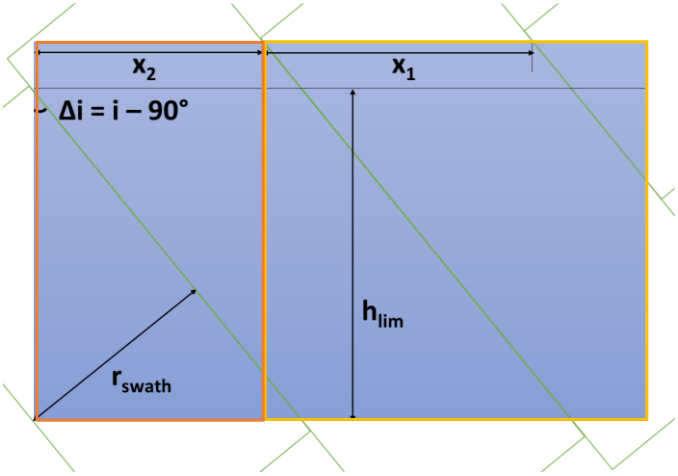

Figure 3: AOI coverage from four ascending beams for $h_{\text{AOI}} > h_{\text{lim}}$. For illustration purposes, the incidence is steeper than in the example shown in Figure 2.

b) Mixed Acquisition Direction Coverage

Various other SAR applications on the other hand, provide the opportunity to exploit the complementary information obtained from different viewing geometries as described in [27] and [28]. For the coverage estimation this means that ascending and descending acquisitions can be combined and that in general the AOI can be covered faster in comparison to exclusively using only one of the two directions. It might lead to a higher total number of acquisitions since the effective coverage area of ascending and descending beams is lower than using only one acquisition direction. Nevertheless, the coverage duration still improves significantly by combining both acquisition directions.

For the determination of the least number of required acquisitions, various potential configurations of ascending and descending beams were analyzed. As the intersections between the beams of both directions reduce the effective coverage area, an optimal coverage is achieved by alternating as little as possible between the ascending and descending beams. An exemplary scenario for such a coverage is shown in **Figure 4** in which two ascending beams cover the left side and two descending beams cover the right side of the AOI.

As the parameters x_1 to x_3 between the single beams and the AOI do not change with regard to the coverage performed from a single direction, as shown in **Figure 2**, the expressions in (1), (2) and (5) remain applicable. Therefore, we can use these parameters to derive the number of required acquisitions from the configuration in **Figure 4**. It can be seen that both, the first

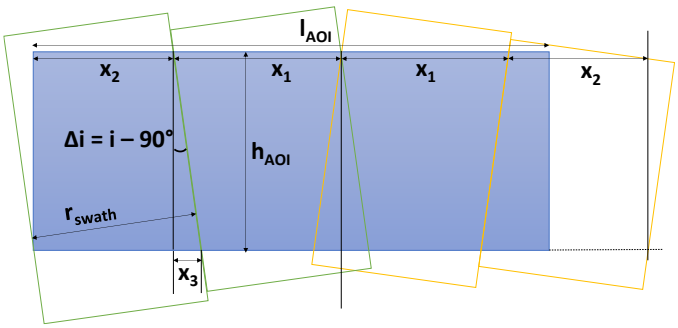

Figure 4: AOI coverage performed from two ascending (green) and two descending orbits (yellow).

beam and the last beam, cover an effective length of x_2. The remaining beams in between those two beams, independent from the direction, cover an effective length in multiples of x_1. In this case the number of required acquisitions for a mixed direction coverage is obtained from:

$$n_{\text{acq,mixed}} = \left\lceil \frac{l_{\text{AOI}} - 2 \cdot x_2}{x_1} + 2 \right\rceil \text{ for } h_{\text{AOI}} < \frac{r_{\text{swath}}}{2 \cdot \sin \Delta i} \qquad (7)$$

In order to provide an example, an AOI with l_{AOI} = 80 km and h_{AOI} = 40 km is covered by the TerraSAR-X satellite with r_{swath} = 24 km in Stripmap mode and i = 97.44° [29]. In this case x_1 results to 24.2 km and x_2 to 18.98 km and therefore $n_{\text{acq,mixed}}$ results to four. This means that two acquisitions in ascending and two in descending direction are needed to cover the AOI.

Similar to the single direction coverage the expression in (7) is only applicable if h_{AOI} does not exceed a certain height limit which is annotated in (7). In contrast to the definition in (3), exceeding this height limit, referred to as $h_{\text{lim,mixed}}$, does not generate unreasonable outcomes but changes the effective coverage area of the beams covering the right side of the AOI. This is illustrated in **Figure 5**.

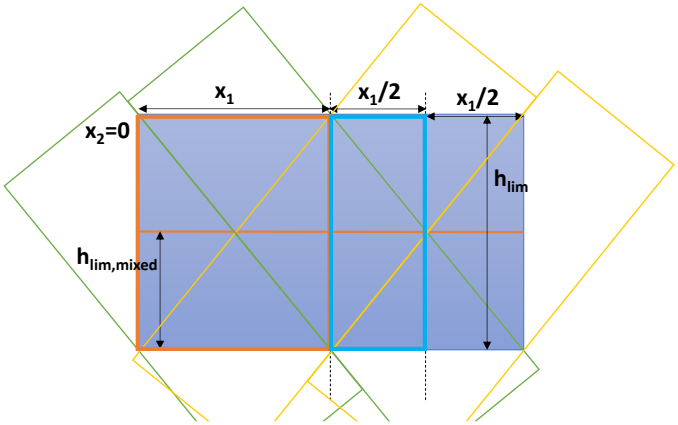

Figure 5: AOI coverage performed by four mixed beams for $h_{\text{AOI}} > h_{\text{lim,mixed}}$.

It can be seen that when h_{AOI} becomes greater than h_{lim} the situation that was described in **Figure 4** starts to repeat. Therefore, we can first extend the expressions in (7) for all h_{AOI} that are not in between $h_{\text{lim,mixed}}$ and h_{lim} to:

$$n_{\text{acq,mixed}} = \left\lceil \frac{l_{\text{AOI}} - 2 \cdot x_2}{x_1} + 2 \cdot \left\lceil \frac{h_{\text{AOI}}}{h_{\text{lim}}} \right\rceil \right\rceil \quad (8)$$

for $(h_{\text{AOI}} \,\%\, h_{\text{lim}}) < h_{\text{lim,mixed}}$

Furthermore, it is shown that for AOIs with an h_{AOI} in between $h_{\text{lim,mixed}}$ and h_{lim}, the first beam has an effective coverage length of x_2, the second and all following beams in the same acquisition direction of x_1. All beams that are oriented in a different direction yet have an effective coverage length of $0.5 \cdot x_1$. In this case it is not possible to provide an analytical solution to find the best combination of ascending and descending beams with the least number of acquisitions. Instead, these situations are solved in an iterative optimization process. Using the outcome of (8) as a starting point for the number of acquisitions, different combinations of ascending and descending beams are evaluated for the coverage. If a combination with this number of acquisitions is found that provides a coverage of the AOI, the number of acquisitions is reduced by one. Then the evaluation of ascending descending combinations is performed again. This process is repeated until no coverage is possible anymore. The number of acquisitions of the last possible coverage is then used as $n_{\text{acq,mixed}}$.

B. Beams with Fixed Incidence Angle Ranges

Common SAR systems use phased array antennas and electronically steer the beams over the available incidence angle range of the antenna which is described in [30]. The number of available beams and the swath width vary according to the different modes, e.g. Stripmap or ScanSAR, that can be applied [31]. These modes use a fixed incidence angle range for each beam [32] which means that they cannot be continuously moved over the entire incidence angle range of the antenna. Hence, the location of an AOI needs to be considered when determining the number of required acquisitions and (6) as well as (8) need to be adapted.

As analyzing the discrete incidence angle range for each mode and considering various AOI positions requires information that might not be available in early mission phases, the deviation from the optimal number of acquisitions is approximated. We therefore define a worst-case scenario that maximizes the number of required acquisitions. For this purpose, we derive the according worst-case AOI location from the optimal case which was displayed in **Figure 2** and **Figure 4**. For an ascending, right-looking beam this is when the far-range side of the beam intersects with the westward upper edge of the AOI, as displayed in **Figure 6**. For a descending, right-looking beam it is when the near-range side intersects with the westward lower AOI edge. These positions allow to completely cover the latitude extent of the AOI while only covering the minimum fraction of the longitude extent. They therefore maximize the number of required beams.

Comparing the configuration and considering the AOI latitude extent l_{AOI}, for example between **Figure 2** and **Figure 6**, we derive that the maximum number of required acquisitions can only increase by plus one compared to the optimum number of acquisitions $n_{\text{acq,single}}/n_{\text{acq,mixed}}$. If two additional acquisitions were required from this position to cover l_{AOI}, then also $n_{\text{acq,single}}/n_{\text{acq,mixed}}$ increases by plus one. The difference between optimum and maximum number of acquisitions then remains the same. From this observation the maximum of this number for both single and mixed acquisition direction is derived to:

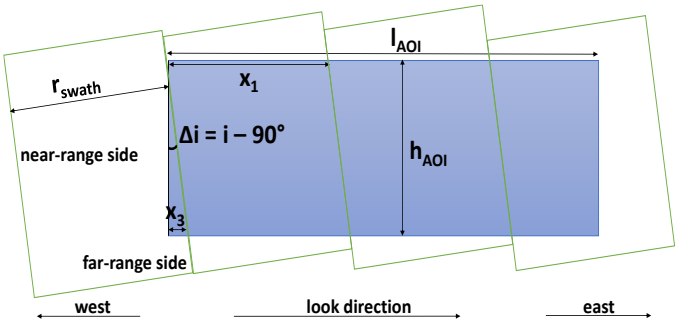

Figure 6: AOI coverage performed from four ascending (green) orbits in a configuration that maximizes $n_{\text{acq,single}}$.

$$n_{\text{acq,max}} = n_{\text{acq}} + 1 \quad (9)$$

for both single and mixed acquisition direction coverage

C. Average Effective Coverage Range

As mentioned before, due to the inclination and the fixed orientation of the AOI in latitude and longitude, the beams are not parallel towards the latitude extent of the AOI. Furthermore, we have seen that the range in latitude that one beam covers, is not constant. It depends on the height of the AOI as well as on which beam is considered. We therefore compute the average range that can be covered from all used beams, considering the number of required acquisitions and also the height of the AOI. In this way we can determine the average range a swath can cover, i.e. the average effective coverage range. It is applicable to all the required beams which is required when computing the accessibility to the AOI, which means to determine the number of orbits that have access to the AOI at given latitude. This is elaborated in the following section chapter III.

According to (6) and (8) the expressions are defined separately for the use of either single and mixed acquisition directions. By summarizing the individual coverage ranges x_1 and x_2 from the utilized beams, the average effective coverage range is obtained from:

$$r_{\text{cov,single}} = \frac{(n_{\text{acq,single}} - \left\lceil \frac{h_{\text{AOI}}}{h_{\text{lim}}} \right\rceil) \cdot x_1 + x_2}{n_{\text{acq,single}}} \quad (10)$$

$$r_{\text{cov,mixed}} = \frac{(n_{\text{acq,mixed}} - 1 - \left\lceil \frac{h_{\text{AOI}}}{h_{\text{lim}}} \right\rceil) \cdot x_1 + 2 \cdot x_2}{n_{\text{acq,mixed}}} \quad (11)$$

For mixed acquisition directions that cover an AOI with a h_{AOI} that is in between $h_{\text{lim,mixed}}$ and h_{lim}, as described in the previous section, the distribution of the number of ascending n_{asc} and descending beams n_{desc} is determined in an optimization process. By using the individual beam coverages as shown in **Figure 5**, the average effective coverage range $r_{\text{cov,mixed}}$ in these cases is derived to:

$$r_{\mathrm{cov,mixed}} = \frac{\left(n_{\mathrm{asc}} - \left\lfloor \frac{h_{\mathrm{AOI}}}{h_{\mathrm{AOI,lim}}} \right\rfloor\right) \cdot x_1 + x_2 + n_{desc} \cdot \frac{x_1}{2}}{n_{\mathrm{acq,mixed}}} \qquad (12)$$

for $h_{\mathrm{lim,mixed}} < (h_{\mathrm{AOI}} \,\%\, h_{\mathrm{lim}}) < h_{\mathrm{lim}}$

With (10) to (12) the average effective coverage range is defined for all possible scenarios. As an example, we compute the average effective coverage range for an AOI with h_{AOI} = 40 km and l_{AOI} = 50 km for an inclination of i = 97.44°. In a single direction coverage with a swath width of r_{swath} = 24 km, this AOI requires $n_{\mathrm{acq,single}}$ = 3 acquisitions. In this case, the average effective swath coverage yields 25.6 km, differing from the effective swath width by 1,6 km. This adjusted coverage information will be used in the following for a more precise determination of the accessibility to an AOI.

III. AOI Accessibility

The most commonly used orbits for Earth observation with SAR are sun-synchronous repeat ground-track dawn/dusk orbits. This has multiple advantages such as the maximized exposure duration of the solar panels to sunlight, optimized stability of the thermal environmental conditions as well as global coverage capability at almost all latitudes [17]. Furthermore, the repeating ground-tracks ensure an identical viewing geometry in every repeat cycle which is a key advantage in applications such as repeat-pass interferometry [33]. Additionally, the distance between the orbital ground-tracks is largest at the equator and gradually decreases towards the poles [34]. As a result, acquisitions from higher latitudes gain increased accessibility to an AOI because the AOI is visible from a higher number of orbits than in lower latitudes. The process to determine the number of these orbits at a given latitude is described in the following chapters focusing on how to quantify the overlap and the role of the location of the AOI. This results in the determination of the number of orbits from which the AOI is accessible being the key aspect of this chapter for the further coverage duration estimation.

A. Overlapping Orbit Access Ranges

The distance between the ground-tracks of the orbits on the equator is characteristic for every sun-synchronous repeat ground-track orbit (SSO). This so-called minimum interval is obtained by dividing the circumference of the Earth at the equator by the total number of revolutions around the Earth in one full repeat cycle R [17]. In order to achieve a complete and gapless global coverage the incidence angle range of a SAR system, in the following referred to as access range (AR), is required to stretch at least over the entire minimum interval as explained in [18] and [35]. In general, the size of the AR r_{AR} depends on the size and the design of the antenna as well as on the desired performance. Due to stronger range and azimuth ambiguities for steep and shallow incidence angles, usually not the entire feasible AR is used as explained in [32]. Instead, a smaller range is chosen for which the performance meets the criteria of the mission requirements. In the case of TerraSAR-X for example, the accessible incidence angle range of the antenna reaches from 15° to 60° but the full performance range

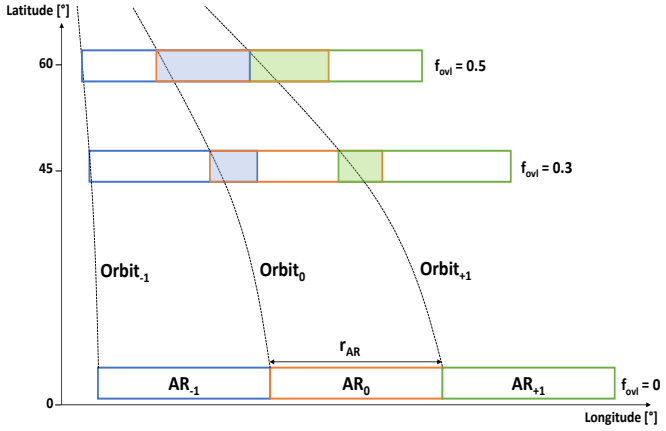

Figure 7: Overlapping ARs and decreasing distance between ground-tracks towards the north pole, shown for three orbits.

is defined from 20° to 45° which translates to eleven Stripmap beams with an AR of 264 km [32]. As the minimum interval for TerraSAR-X orbit is 240 km, this creates an initial overlap between two adjacent ARs at the equator of $r_{\mathrm{ovl},0}$ = 24 km.

As r_{AR} only depends on the defined incidence angle range of the SAR system, hence does not vary over the latitude, the ARs between adjacent orbits begin to increase their overlap with absolute increasing latitude Λ. In those overlapping ranges an access to a potential AOI can be achieved from multiple orbits which is displayed in **Figure 7**. Please note that r_{AR} variations due to variations in the orbit altitude are neglected.

The extent of the overlap is in the following characterized by the overlap factor f_{ovl}. This factor can be approximated assuming equidistant spacing between the ground-tracks of the orbit. As a result, it is only applicable to orbits with a repeating ground-track pattern such as SSOs. For other orbit types the overlap factor has to be adjusted to the respective ground-track pattern otherwise resulting in false evaluation of the overlap. By comparing the distance in longitude direction between two adjacent ground-tracks on the equator d_{e} with the according distance at the given latitude d_Λ, f_{ovl} can then be quantified. The distance on the equator d_{e} is obtained by dividing the circumference of the earth on the equator by the number of revolutions R in one repeat cycle whereas d_Λ is obtained by dividing the circumference of the earth at the given latitude by R. Therefore, d_Λ can be expressed by means of d_{e} and the cosine of the latitude. The overlap factor then results to:

$$f_{\mathrm{ovl}} = \frac{d_e - d_\Lambda}{d_e} = 1 - \cos\Lambda \qquad (13)$$
$$\text{with } d_\Lambda = d_e \cdot \cos\Lambda$$

With f_{ovl} it is then possible to derive the range of the overlaps $r_{\mathrm{ovl},n}$ of the ARs of all adjacent orbits. As depicted in **Figure 7**, a central orbit n = 0 with a central access range AR_0 (orange) is chosen for which the overlap range in positive (+n) and negative (-n) longitude direction is analyzed. As the overlap is identical between all ARs and their respective neighbors, any orbit is suitable to be chosen as the central orbit of the analysis. From this orbit with n = 0, the overlap range of the orbit ±n is then obtained from:

$$r_{\mathrm{ovl,n}} = r_{\mathrm{AR}} \cdot \left(|n| f_{\mathrm{ovl}} - (|n| - 1)\right) + |n| \cdot r_{\mathrm{ovl,0}} \qquad (14)$$
$$n = \pm 1, 2, \ldots, R$$

For example, for the adjacent orbits displayed in **Figure 7** with $n = \pm 1$, the overlap range yields $r_{\mathrm{ovl,1}} = r_{\mathrm{ovl,-1}} = f_{\mathrm{ovl}} \cdot r_{\mathrm{AR}} + r_{\mathrm{ovl,0}}$. Due to the absolute value of n in (14) both overlap ranges in positive and negative longitude direction are identical. Further details in case $r_{\mathrm{ovl},n}$, for example for $n = \pm 2$ at $\Lambda = 0°$, becomes negative will be provided in section III.C.

B. AOI Location

In this section the visibility of an AOI at a given latitude is analyzed from the adjacent orbits in combination with the overlap determined in the preceding section. This results in a maximum number of orbits that can be used to cover the AOI. Due to the overlapping ARs, which are displayed in **Figure 7**, and the extent of the AOI in longitude direction, an AOI might be located within the AR of one orbit in such a way, that it can be accessed from multiple adjacent orbits. This means that these locations provide the highest number of access possibilities thus the fastest coverage duration for the given latitude. From (13) it is obvious that the higher the absolute value of the latitude Λ, the higher the overlap factor and hence the higher the probability of a multiple access. However, analyzing multiple accesses only makes sense if the AOI requires at least two beams to be completely covered. Otherwise the location is irrelevant as the AOI can be acquired with only one acquisition by any orbit with an access. Hence the following considerations refer to AOIs that are larger in longitude than the effective swath width of the system.
In order to identify the locations within the AR of a central orbit that enable the AOI to be accessible from multiple orbits, we analyze potential AOI locations considering the overlap and the length of the AOI. For this purpose, **Figure 8** shows a simple scenario of one central AR (AR_0 in orange) and two adjacent overlapping ARs (AR_{-1} in blue and AR_{+1} in green). The overlap on each side is characterized by $r_{\mathrm{ovl},\pm1}$.

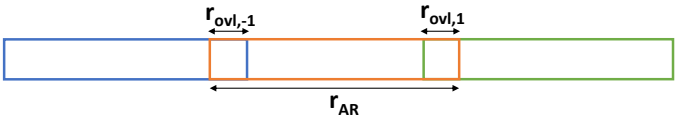

Figure 8: Overlapping scenario of one central orbit AR (orange) and two ARs from the adjacent orbits (blue and green).

In this scenario it can be seen that an AOI can potentially be accessed from two ARs (either blue and orange or orange and green) at the same time. The according AOI locations are shown in **Figure 9**. By defining a coordinate system, we determine the exact locations that provide the opportunity for a given AOI to be accessed from the neighboring orbits. In **Figure 9** this is visualized with $r_{1,\min}$ as the western limit for a potential AOI location which grants access from AR_{-1} and AR_0 and $r_{1,\max}$ as the according eastern limit. The same is shown for $r_{2,\min}$ and $r_{2,\max}$ as the respective limits for a simultaneous AOI access from AR_0 and AR_{+1}. The first index enumerates the overlapping adjacent ARs from left to right i.e. from negative to positive latitude direction and the second index if the according location is closer to the origin of the coordinate system.

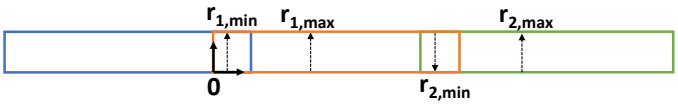

Figure 9: AOI location limits that enable an access to the AOI from two adjacent orbits (either orange and blue or orange and green).

It can be seen that from the two positions $r_{1,\min}$ and $r_{2,\max}$ at least one part of an AOI is covered from the central orbit (orange) and the remaining part is covered from an adjacent orbit (blue or green). Furthermore, for the two positions $r_{1,\max}$ and $r_{2,\min}$ this is reversed and at least one part is covered from an adjacent orbit while the remaining part is covered from the central orbit. In summary this means if the AOI is located between the min and max positions of each index pair, referred to as r_1 and r_2 in this case, an access from both the central and one adjacent orbit is enabled. This is shown along with exemplary AOI locations at the outer limits of r_1 and r_2 in **Figure 10**. For the locations (a) and (b) maximum one acquisition can be performed from the central orbit (orange). The locations (c) and (d) allow maximum one acquisition from one of the adjacent orbits (blue for (c) and green for (d)).
From **Figure 9** and **Figure 10** it can be seen that in order to quantify the parameters $r_{1,\min}$ to $r_{2,\max}$ obviously the extent of the AR and the average effective coverage range but also the overlap $r_{\mathrm{ovl},n}$ as well as the AOI length l_{AOI} have to be considered. For higher overlaps $r_{1,\max}$ is shifted further in the positive direction i.e. eastward and $r_{2,\min}$ is further shifted westward. An example is shown in **Table 1**. For an increasing l_{AOI}, $r_{1,\max}$ but also $r_{2,\max}$ are shifted eastwards.
In this case it might be concluded that also $r_{1,\min}$ is shifted eastwards. However, the shift direction for this position strongly depends on the size of the l_{AOI} increase. The determination of the position of $r_{1,\min}$ is based on the relation between the swath width and the length of the AOI. In the above illustration in **Figure 9**, it specifies the location at which maximum one acquisition can be performed from AR_0 while the remaining ones have to be performed from AR_{-1}. Moving the AOI further west would mean, that an acquisition from AR_0 does not contribute anymore to minimizing the duration to cover the AOI. Although the AOI is still accessible from AR_0, the number of required acquisitions then has to be performed entirely from AR_{-1}. Thus in other words, $r_{1,\min}$ defines the minimum part of an AOI that needs to be accessible by one orbit, so that an acquisition from this orbit reduces the number of acquisitions from the adjacent orbits.
Looking again at **Figure 9**, one can see that the distance between the position $r_{2,\min}$ and the western end of AR_1 (green) is identical to $r_{1,\min}$. As this applies to all $r_{j,\min}$ and the western limit of their respective ARs, the parameter $r_{1,\min}$ is generalized. It will therefore be referred to as $r_{\min}$ in the following. Based on the geometry of the overlapping ARs, the length l_{AOI} and the average effective coverage range for single or mixed acquisition directions r_{cov}, $r_{\min}$ is derived to:

$$r_{\min} = l_{\mathrm{AOI}} - \left(\left\lceil \frac{l_{\mathrm{AOI}}}{r_{\mathrm{cov}}} \right\rceil - 1\right) \cdot r_{\mathrm{cov}} \tag{15}$$

With $r_{\min}$ and the overlap range obtained from (14) it is then possible to determine the geometric parameters ($r_{1,\min}$ to $r_{2,\max}$).

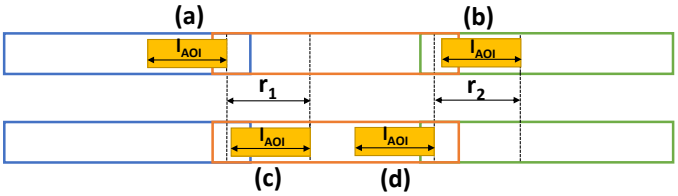

Figure 10: Exemplary AOI positions at the outer limits of r_1 and r_2 that enable an access from the ARs of two adjacent orbits. In the upper plot for (a) and (b) maximum one acquisition is performed from the center orbit while in the lower plot for (c) and (d) maximum one acquisition is performed from an adjacent orbit (blue or green).

Considering all possible adjacent orbit overlaps these parameters are eventually generalized to:

$$r_{j,\min} = r_{\mathrm{AR}} + r_{\min} - r_{\mathrm{ovl},j-1} \tag{16}$$

$$r_{j,\max} = l_{\mathrm{AOI}} - r_{\min} + r_{\mathrm{ovl},\alpha-j} \tag{17}$$

$$r_j = r_{j,\max} - r_{j,\min} \tag{18}$$

$$j = 1, 2, \ldots, n_{\mathrm{o}}$$

For better readability, the parameter α in (17) is used as a substitute for the maximum number of orbits n_{o} that provide a possible access to the AOI. This number is obtained in an iterative process including $r_{\min}$ as well as the adjacent overlaps. As the derivation of the according iteration criterion is based on the preceding geometric consideration, it is explained in detail in the subsequent section.

As an example for a single direction coverage, using the scenario which is displayed in **Figure 8**, the maximum number of orbits with an access is set to $n_{\mathrm{o}} = \alpha = 2$. For a given AOI extent of l_{AOI} = 50 km, and h_{AOI} = 40 km, an AR of r_{AR} = 240 km and an average effective coverage range r_{cov} = 25.6 km, the results for the geometric parameters at different latitudes are shown in **Table 1**. The parameter $r_{\min}$ in this case yields 24.4 km. It can be seen that with higher latitudes, the overlapping area hence the range in which an access from two orbits becomes possible, increases.

Table 1: Overlap and geometry parameters at different latitudes for $n_{\mathrm{o}} = 2$, l_{AOI} = 50 km, r_{cov} = 25.6 km and r_{AR} = 240 km.

Λ [°]	$r_{\mathrm{ovl},1}$ [km]	$r_{1,\min}$ [km]	$r_{1,\max}$ [km]	$r_{2,\min}$ [km]	$r_{2,\max}$ [km]
0	0	24.4	25.6	264.4	265.6
15	8.2	24.4	33.8	256.2	265.6
30	32.2	24.4	57.8	232.2	265.6
45	70.3	24.4	95.9	194.1	265.6
58	102.3	24.4	128.0	162.0	265.6

C. *Determination of the Number of Orbits with AOI Access*

In terms of determining the coverage duration, the key conclusion from the preceding considerations is denoted by the maximum number of orbits with a potential AOI access n_{o}. If higher numbers of n_{o} are achieved this means, that a coverage is performed with a higher number of orbits which in turn decreases the coverage duration. Higher n_{o} are usually achieved for higher latitudes (> 50°). If n_{o} is lower, less orbits can access the AOI and thus the coverage duration increases.

In order to determine n_{o}, the results of (13) – (18) are evaluated iteratively for each adjacent orbit until n_{o} is obtained. A first general overview of n_{o} can be provided by plotting the ARs of multiple orbits over the entire latitude range and analyze their overlap regions. This is demonstrated in **Figure 11** with the according number of access possibilities for a central orbit (orange) and two adjacent orbits in positive (green and black) and negative (yellow and blue) longitude direction. It can be seen that the accessibility increases towards the poles until all five adjacent orbits are able to access a potential AOI.

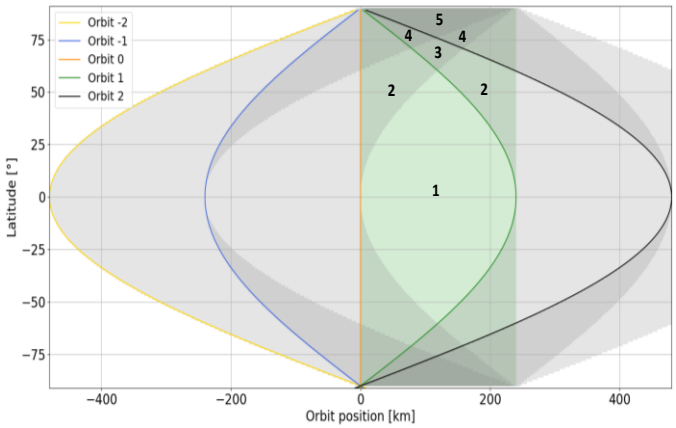

Figure 11: Overlapping orbit ARs with number of possible orbits that have an access to an AOI shown for five adjacent orbits.

Aiming at a more precise determination of n_{o} it is important to evaluate the AOI accessibility from the adjacent orbits with absolute increasing latitude. Particularly interesting are the latitudes in which the number of orbits from which the AOI can be accessed is about to change and n_{o} is about to increase by one. Therefore, we analyze the accessibility of the AOI from the ARs of $\pm i$ in positive and negative longitude direction, at latitudes that provide the opportunity to increase n_{o}. Based on the scenario in **Figure 8**, **Figure 12** shows an example for a such a potential situation at Λ = 54°.

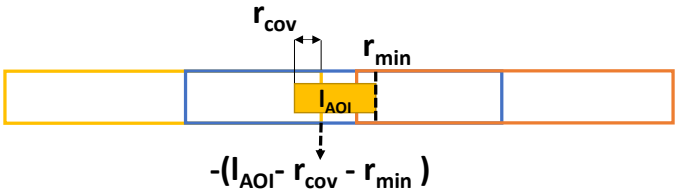

Figure 12: AOI locations and overlap at Λ=54° close before the AR from orbit n = -2 (yellow) and n = 0 (orange) begin to overlap.

At this latitude the subsequent AR_{-2} from orbit n = -2 (yellow) is getting close to overlapping with AR_0 of the central orbit (orange). If the distance between AR_0 and AR_{-2} is small enough, the AOI can then also be accessed from the orbit n = -2. Hence the proportion of an access to an AOI from the next adjacent orbit becomes greater than zero and therefore n_o increases by one. Considering the length of the AOI l_{AOI} and employing the geometric considerations in **Figure 12**, we establish a criterion for the overlap obtained from (14) at which an increase of n_o occurs:

$$r_{ovl,n} \geq -(l_{AOI} - r_{cov} - r_{min}) \tag{19}$$

With this criterion the overlaps of the adjacent ARs are iterated. Whenever an overlap meets the condition n_o is increased. If it fails the iteration is stopped and n_o is eventually obtained. This process is illustrated schematically in **Figure 13**.

For the remaining positions along AR_0 for which n_o cannot be achieved, we define a minimum number of orbits with AOI access n_o'. This number is simply obtained by:

$$n_o' = n_o - 1. \tag{20}$$

If for example n_o = 2 then n_o' which has access to the entire AOI results to 1.

As explained in section III.B, n_o can only be achieved for certain AOI locations along AR_0. Otherwise the AOI can only be covered by n_o'. The according locations between which n_o is achieved, are defined as ranges in (18). In order to make a statement about the likelihood of an AOI to be accessed from n_o, we derive the proportion p_α of the AOI to be located within these ranges against all possible locations of the AOI. In (17)

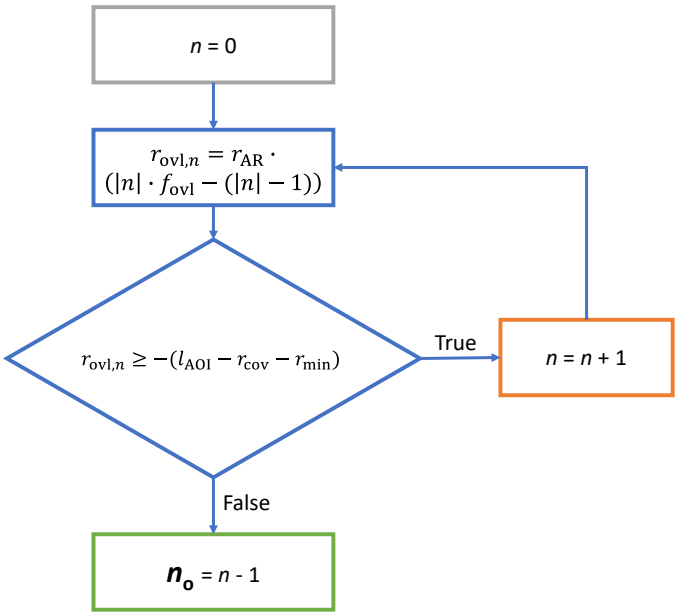

Figure 13: Iteration of the expression in (19) to obtain the maximum number of orbits with an access to an AOI n_o.

the index α is introduced as a substitute for n_o for reasons of better readability. For the proportion, we compute the sum over all ranges obtained from (18) and divide it by the maximum range in which the AOI can potentially be located and still be accessible from AR_0:

$$p_\alpha = \frac{\sum_{j=1}^{\alpha} r_j}{r_{\alpha,\max} - r_{\min}} \tag{21}$$

for $r_{ovl,n} < -(r_{AOI} - 2 \cdot r_{min})$

This expression returns accurate results for overlaps within the range of $r_{ovl,n} \leq -(r_{AOI} - 2 \cdot r_{min})$ where $p_\alpha \leq 1$. As the overlap approaches this limit, the expression in (21) needs to be extended in order to obtain the correct proportion for n_o. Otherwise the proportion would become greater than one when the limit is exceeded. The reason is that $r_{j,max}$ (17) then becomes greater than $r_{j+1,min}$ (16) before the overlap is big enough to fulfil the criteria in (19). As a consequence, the sum of r_j becomes then greater than the AR before the next higher number of orbits with an access is reached. In the example in **Figure 12**, in such a situation the AOI can be covered by AR_{-1} (blue) and either by AR_{-2} (yellow) or by AR_0 (orange) but not by all three ARs at the same time. Therefore, the proportion for a coverage from n_o = 2 remains at one. In order to counteract false proportion results, we therefore set the proportion to one, for all overlaps between the limit in (21) and the criteria in (19).

$$p_\alpha = 1 \tag{22}$$

for $-(r_{AOI} - 2 \cdot r_{min}) \leq r_{ovl,n} < -(r_{AOI} - r_{min} - r_{cov})$

With the adjusted proportion and by performing a numerical analysis of $r_{ovl,n}$ over the entire latitude range, the global distribution of n_o (**Figure 14** top) and the according proportion p_α (**Figure 14** bottom), can be visualized. This is shown for an ascending viewing direction with the TerraSAR-X orbit parameters and the according swath width r_{swath} = 24 km in Stripmap mode in **Figure 14**. The dimensions of the AOI are l_{AOI} = 100 km and h_{AOI} = 40 km, respectively. It becomes apparent that the impact of the overlap increases rapidly starting from Λ = ±50° towards the poles. As the maximum achievable number of orbits at the highest latitude also depends on the size of the AOI, the depicted maximum is variable. In general, this maximum is higher for greater AOI sizes as they are accessible from more orbits than smaller AOIs at the same latitude.

By reason of the inclination, the satellite's ground-track is limited to a certain latitude range depending on the inclination difference Δi towards 90° and the maximum inclination of the antenna beam. The inclination limit can be obtained by determining the maximum slant range of the SAR system and translate the result into the according latitude as mentioned in [36]. For simplification, in the following examples we chose the maximum latitude of the orbit ground-track of TerraSAR-X with 82.6°. This explains the white fringes that appear at the top and bottom of the global map in **Figure 14**.

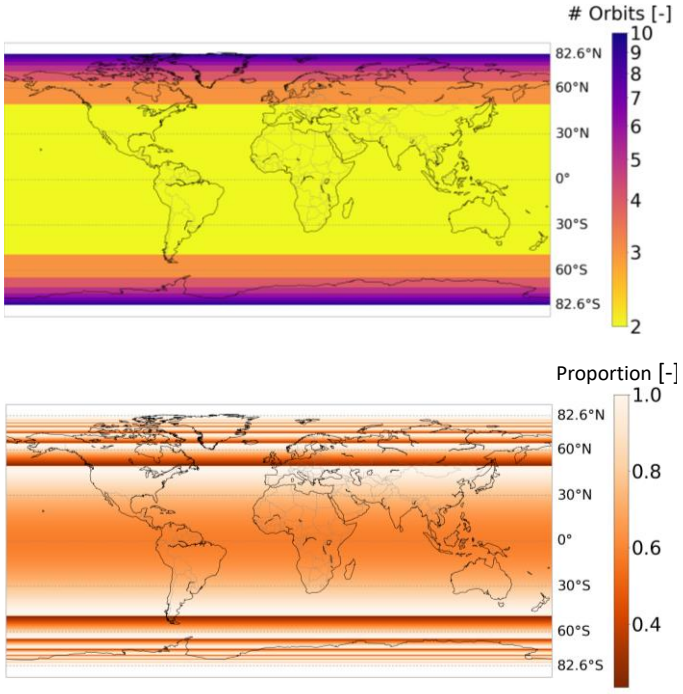

Figure 14: Globally distributed number of orbits n_o with an access to the AOI (top) and the according global proportion distribution p_α (bottom), for l_{AOI} = 100 km, h_{AOI} = 40 km for the TerraSAR-X orbit from an ascending viewing direction.

D. Distribution of the Number of Required Acquisitions between Number of Orbits with an Access to the AOI

The previous sections have shown how to determine the number of orbits from which an AOI is accessible at a certain latitude. Now for the further coverage duration computation it is important to know, how the acquisitions are distributed between these orbits. In general, an equal distribution for which all orbits in n_o can perform the same number of acquisitions, will achieve the best results in terms of coverage duration. However, this is not always feasible. In order to determine which distribution is applicable we therefore analyze how many acquisitions can be performed from each orbit in n_o. For this purpose, we assume that the center of the AOI is located in the center of the central AR, as illustrated in **Figure 15**. In this way, we can assure that the adjacent orbits to the west and east of the central AR can cover the same fraction of the AOI. From this configuration we then compute the number of acquisitions which can be performed from the outer orbits. Derived from geometric relation as illustrated in **Figure 15** the parameter $n_{acq,outer}$ is expressed as:

$$n_{acq,outer} = \frac{0.5 \cdot r_j + r_{\min}}{r_{cov}} \qquad (23)$$

Since the AOI in this case is located in the center of the central AR, the configuration is axisymmetric, visible in **Figure 15**, and therefore any r_j according to (18) can be used in (23).

By multiplying $n_{acq,outer}$ with the number of orbits n_o and comparing the outcome to the number of required acquisitions $n_{acq,single}/n_{acq,mixed}$, we can evaluate if the distribution of acquisitions between the orbits is equal or imbalanced. In case of an equal distribution, which happens when $n_{acq,outer} \cdot n_o \geq n_{acq,single}/n_{acq,mixed}$, the AOI can be covered from all orbits in n_o with the same number of acquisitions and we directly proceed to the coverage duration determination. In case of an imbalanced distribution a minor part of the AOI is covered from the adjacent orbits while the major part is covered from the center orbit. In terms of coverage duration this means the coverage from the central orbit is the dominating factor. Therefore, we first determine the number of acquisitions that are needed from the central orbit and then consider only the central coverage for the further coverage duration determination.

Please note that these considerations only have to be made for n_o. For n_o' the acquisitions can always be distributed equally between the orbits.

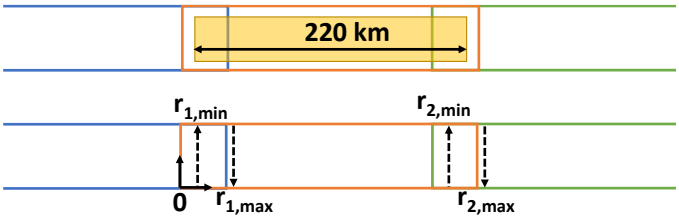

Figure 15: AOI with l_{AOI} = 220 km located in the middle of the central AR (orange) at Λ = 38°. In this configuration, only a small fraction of the coverage can be performed from the adjacent ARs (blue and green) while the major coverage is performed form the central AR.

E. Angular Beam Separation between adjacent Orbits

In chapter II the number of required acquisitions to cover an AOI was derived assuming all used beams are parallel to each other. This is of course true for the beams from only one orbit and also for an AOI coverage on the equator. However, the analysis of the increasing overlap between the ARs from adjacent orbits revealed, that as the ground-tracks of the orbits reduce their distance with increasing latitude, also the alignments of the beams between the adjacent orbits change. As a consequence, gaps appear between the beams of adjacent orbits which increase in size towards the poles. Furthermore, the effect intensifies for increasing Δi as well as for increasing AOI dimensions. The actual coverage thus requires more beams for the complete AOI coverage than estimated in chapter II as the AOI moves further away from the equator.

A solution to overcome these increasing gaps would be to include the angular separation of the adjacent beams in the computation of the required number of acquisitions. However, this involves a more precise and detailed knowledge of the satellite's orbit parameters and more over increases the complexity of determining the most effective distribution of acquisition, in particular in the mixed acquisition direction case. Instead it is also possible to add a margin of additional acquisitions to coverages at higher latitudes. A general margin can be derived by including the maximum number of orbits with a potential AOI access n_o to consider all gaps between the involved orbits, as well as the AOI length in longitude l_{AOI}. To also include the orbit characteristics, furthermore the distance S_D between two adjacent obits at the equator, also referred to as

minimum interval, is considered. This margin is then depending on the latitude in which the AOI is analyzed as the gaps become wider towards the poles. **Table 2** therefore shows the margin that needs to be added to both single and mixed direction coverages at different latitude ranges. For latitudes below a certain threshold, no margin needs to be added as the beams are almost parallel and the gaps in this latitude range can be neglected. We define this threshold as the latitude until which the angular difference between the inclination of the ground-track of the satellite and the inclination of the orbit is less than 1°. Taking TerraSAR-X as an example, this threshold is reached at a latitude of approximately 20°. For latitudes above this threshold, the margins are applicable if n_o is larger than two. Otherwise the influence of the gaps is too small and can be neglected.

Table 2: Margins to add to the number of required acquisitions for both ascending and descending orbits at different latitude thresholds that are applicable to the TerraSAR-X satellite.

Latitude	**Margin added to n_{acq}**
$\Lambda < 20°$	+ 0
$20° \leq \Lambda \leq 50°$	$+ \left\lfloor \frac{n_o}{2} \right\rfloor$ (for $n_o > 2$)
$\Lambda > 50°$	$+ \left\lfloor \frac{n_o}{2} \right\rfloor + \frac{l_{AOI}}{0.5 \cdot S_D}$

Including these margins has proven to be sufficient to cover the gaps and achieve accurate results. A detailed analysis of the results for the TerraSAR-X satellite can be found later on in **Table 5** when discussing the outcome of the coverage duration determination approach in section IV.C.

IV. Coverage Duration Estimation

By combining the number of required acquisitions to cover an AOI with the number of orbits from which the AOI is accessible, the coverage duration is finally estimated. This is achieved in particular by analyzing the orbit's ground-track pattern in order to determine the time until the satellite has reached the adjacent orbits. The approach is elaborated in the following section. Furthermore, the presented approach is validated by means of planning results from the TerraSAR-X mission. Please note that the approach does not consider the planning system, memory restrictions, the time to reach a downlink opportunity or the time until the first acquisition can be performed. For the coverage duration it is assumed that the first acquisition can be performed instantaneously. The approach therefore approximates the duration between the first and the last required acquisition without considering any pre- or post-processes.

A. Duration Estimation from Sub-Cycle Pattern

a) Single Acquisition Direction Coverage

In order to derive the coverage duration by means of n_o and $n_{acq,single}$ obtained from (6), the time for the satellite to reach the relevant adjacent orbital ground-track needs to be determined. This is accomplished by computing the repeating ground-track pattern of orbits within two consecutive equatorial crossings of the ground track, i.e. within the fundamental interval S_Q. For simplification this pattern will be referred to as sub-cycle in the following. According to [37] the sub-cycles can be obtained for either ascending or descending orbits from the number of days D per repeat cycle and an integer number K that represents the fractional part of the number of orbits completed per day. In mathematical terms this is expressed as $Q = I + K/D$ with Q being the revolutions per day and I being the integer part of Q as described in [35] and [38]. In [37] the sub-cycle pattern around a central orbit ($d = 0$) is expressed as:

$$d = \frac{k + m \cdot D}{K} \tag{24}$$

with d being the number of days to reach the adjacent orbit k and m being an additional integer parameter to provide a single unique solution to the above equation for each k. In addition, d, m and k (all displayed in **Figure 16**) are integer numbers with $k \neq 0$. Within this pattern there is no latitude dependency as it remains constant from the equator over the entire orbit when considering only ascending or descending orbits.

For the TerraSAR-X orbit which was used in the preceding chapters with D = 11 d and K = 2 (I = 15), the resulting sub-cycle pattern is depicted in **Figure 16**. The Figure also annotates the fundamental interval on the equator with S_Q = 2640 km.

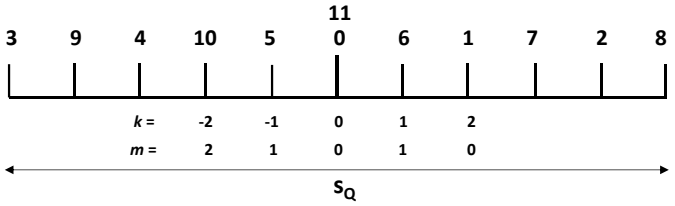

Figure 16: Sub-cycle pattern of ascending orbital ground-tracks for the TerraSAR-X orbit.

Since we cannot specify if an AOI is located left, middle or right to the center orbit, the coverage duration is determined from the sub-cycle pattern by evaluating d for the different orbital ground-track combinations that can be realized with n_o. Given for example the parameters n_o = 3 and $n_{acq,single}$ = 2 to cover an AOI, the resulting combinations of d are [10, 5, 0] days, [5, 0, 6] days and [0, 6, 1] days which is illustrated in **Figure 17** in blue, orange and green.

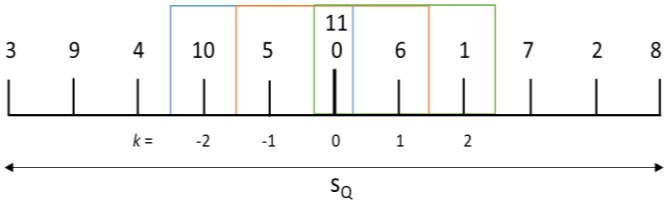

Figure 17: Orbit combinations for TerraSAR-X sub-cycle pattern of ascending orbital ground-tracks for n_o = 3.

For a configuration in which, according to (23), the acquisitions $n_{acq,single}$ are equally distributed between n_o we can obtain the coverage duration by choosing the $n_{acq,single}$-smallest value of d for each of the different combinations and then averaging the results. For the described example with $n_o = 3$ and $n_{acq,single} = 2$ this means that the two lowest values for d are chosen for each combination. This results in [5, 0] days, [5, 0] days, and [0, 1] days. With the maximum value being the determining factor for the coverage duration this results in d_{min} = [5, 5, 1] days. Since it is not possible to say whether the AOI is accessible from the left, middle or right orbit combination, the coverage duration is estimated by averaging the outcome of d_{min} which results in the presented scenario to $\mu(d_{min}) = 3.67$ days where μ represents the average value.

In case $n_{acq,single}$ is higher than n_o the number of required repeat cycles n_{RC} to complete the AOI coverage needs to be added to the previous calculation. They are expressed as:

$$n_{RC,min} = \left\lceil \frac{n_{acq,single}}{n_o} \right\rceil \quad (25)$$

$$n_{RC,max} = \left\lceil \frac{n_{acq,single}}{n_o'} \right\rceil \quad (26)$$

In summary the coverage duration estimation t_{cov} can then be expressed with (25) and (26) as maximum and minimum durations:

$$t_{cov,min} = D \cdot (n_{RC,min} - 1) + \mu(d_{min}) \quad (27)$$

$$t_{cov,max} = D \cdot (n_{RC,max} - 1) + \mu(d_{max}) \quad (28)$$

Given for example $n_{acq,single} = 5$ for the above combinations with $n_o = 3$, means that three acquisitions are performed in the first repeat cycle and the remaining two acquisitions are performed in the second repeat cycle. Therefore, we again choose the second smallest value in the combinations that are highlighted in **Figure 17**. Mathematically this can be expressed by using the modulo operator $n_{acq,single}$ % $n_o = 2$. The acquisitions from the first repeat cycle are going to be considered for the coverage duration determination by n_{RC}. For the minimum coverage duration $t_{cov,min}$ for example, we then have to add $n_{RC,min} = 2$ according to (25). With the expression in (27) this results in an average minimum coverage duration of $t_{cov,min} = 14$ days.

As already mentioned in section III.D, in case the acquisitions are not equally distributed, only the coverage from the central orbit is considered for the determination of the coverage duration. This means in (25) the number of acquisitions for the coverage from the central orbit is used and the number of orbits is set to one.

To provide an overview we evaluated the expression in (25) – (28) for various AOIs over the accessible latitude range and computed the coverage duration for an ascending coverage for l_{AOI} between 40 and 200 km. The results for the maximum coverage duration obtained from (28) are shown in **Figure 18**. As the sub-cycle pattern of single-direction orbits remains constant over the latitude and the central orbit is chosen according to the latitude for which the AOI is analyzed, the results are symmetrical to the equator. Larger AOIs might experience a reduction in coverage duration at lower latitudes than smaller AOIs as they can be accessed earlier from the adjacent ground-tracks due to their size. As a consequence, the coverage of larger AOIs can then be divided between more orbits and therefore the coverage duration can turn out to be lower than smaller AOIs at the same latitude. This is visible in the graph for example between l_{AOI} = 160 km and l_{AOI} = 200 km.

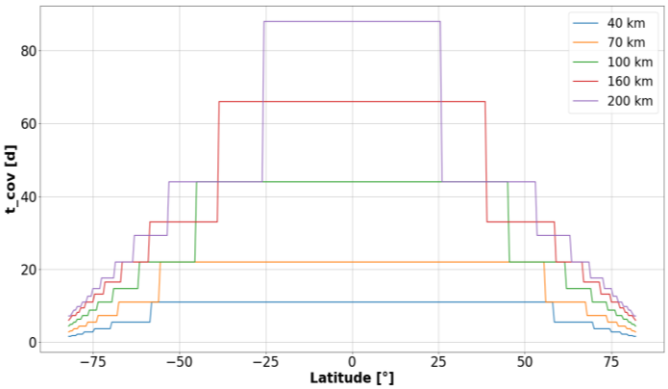

Figure 18: Coverage duration $t_{cov,max}$ for ascending orbits only, estimated for n_o' as well as l_{AOI} = [40, 200] km and h_{AOI} = 40 km between the maximum ground-track latitudes for the TerraSAR-X system.

b) Combined Acquisition Direction Coverage

Coverages that are independent from the viewing geometry, as described in chapter II.A.b), allow the combined use of ascending and descending orbits. In these cases, the sub-cycle pattern as shown in **Figure 16** has to be extended by the sub-cycle pattern of the descending ground-tracks. Furthermore, the determination of d_{min} and d_{max} to solve the expressions in (27) and (28) has to be adjusted accordingly and the number of required acquisitions for the mixed acquisition direction $n_{acq,mixed}$ has to be used in (25) and (26).

In general, the descending sub-cycle pattern on the equator is obtained by calculating the longitudinal shift of the ascending nodes during half an orbit due to the Earth's rotation and the precession of the orbit [39]. Aligning the resulting descending nodes of the orbit with the ascending nodes then yields the combined sub-cycle pattern. Depending on the parameters of the orbit, the equatorial pattern can have two different forms. It can be either coincident when the ascending and descending ground-tracks intersect at the equator, or intermediate when the ascending and descending ground-tracks are uniformly spaced along the equator without crossing each other [40]. In both cases the determination approach of d_{min}/d_{max} is identical. However, in the intermediate case the visual representation of the sub-cycle pattern is shifted towards the east for retrograde and towards the west for posigrade orbits.

Figure 19 displays the orbit combinations for the combined sub-cycle patterns of the TerraSAR-X orbit at $\Lambda = 0°$ (top) and $\Lambda = 33°$ (bottom). As both patterns are coincident the number of nodes at the equator is identical to the single acquisition direction case in **Figure 16**. If the patterns were intermediate the number of equatorial nodes would double and both patterns would be shifted by half the distance between two adjacent orbits $S_D/2$ against each other.

Given the scenario from the preceding chapter with $n_o = 3$ and $n_{acq,mixed} = 2$ at a latitude of $\Lambda = 0°$ (**Figure 19** (top)), the descending ground-track combinations result to [4, 10, 5] days, [10, 5, 0] days and [5, 0, 6] days. The ascending ground-track combinations of d remain unchanged at [10, 5, 0] days, [5, 0, 6] days and [0, 6, 1] days. As even numbers of acquisitions are shared equally between ascending and descending orbits, one acquisition in this case is performed from an ascending orbit while the other one is performed from a descending orbit. Hence the coverage duration for left, middle and right AOI positioning results to d_{min} = [4, 0, 0] days. According to (25) and (27) and by applying $n_{acq,mixed}$ obtained from (8) this then yields a minimum average coverage duration of $\mu(t_{cov,min}) = 1.33$ days.

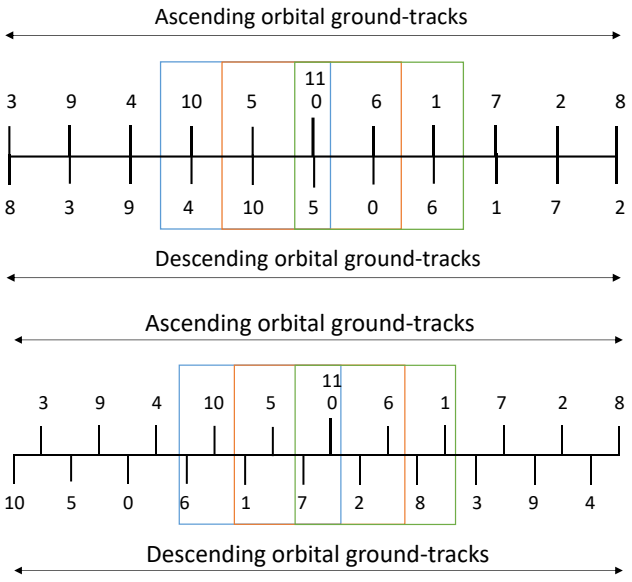

Figure 19: Orbit combinations for TerraSAR-X combined sub-cycle pattern of ascending and descending orbital ground-tracks for $n_o = 3$ at $\Lambda = 0°$ (top) and $\Lambda = 33°$ (bottom).

Similar to the single acquisitions direction we also evaluate the coverage duration obtained from (25) to (28) for multiple AOIs over the accessible latitude range for the mixed acquisition direction case. The outcome of this analysis for $t_{cov,max}$ evaluated for n_o' is shown in **Figure 20**.

Unlike the single-direction pattern, the combined sub-cycle pattern is not constant over latitude. Therefore, only the AOIs that are covered by an odd number of acquisitions are symmetrical to the equator. The last acquisition is then performed in the same direction as the first acquisition. In the case of a first ascending acquisition for example, only the ascending sub-cycle pattern is relevant which is constant over latitude.

The remaining AOIs whose last acquisition is performed in a different direction than the first one, show a fluctuating and asymmetrical coverage duration over latitude. In **Figure 20** these are the AOIs which are covered with a descending beam for the last acquisition. The reason for this behavior is that the descending pattern in this case is not constant in latitude, unlike the ascending pattern. The descending sub-cycle pattern is shifted towards the west against the ascending sub-cycles. This shift can be seen in between $\Lambda = 0°$ (top) and $\Lambda = 33°$ (bottom). For example, towards higher latitudes where multiple ARs are overlapping and the number of orbits with an access to the AOI changes faster with increasing latitude, the coverage duration shows very strong fluctuations.

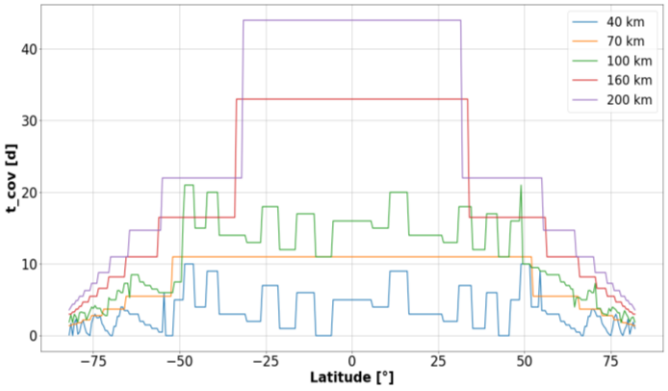

Figure 20: Coverage duration $t_{cov,max}$ for ascending and descending orbits combined, estimated for n_o', l_{AOI} = [40, 200] km and h_{AOI} = 40 km between the maximum ground-track latitudes for the TerraSAR-X system.

B. Coverage Duration Performance Analysis

In early mission phases we generally do not know beforehand which modes are going to be applied or if the SAR system is going to acquire images preferably in single or mixed acquisition direction. Hence, in order to evaluate the coverage capability of the SAR system from a certain orbit, we analyze all potential acquisition scenarios that were previously described and provide an overview by determining the slowest as well as the fastest achievable coverage duration. In the following this is accomplished by determining the coverage duration for a variety of AOIs over the possible latitude range. Included in this analysis is also the consideration of single and mixed acquisition directions as well as different location possibilities or mode specific drawbacks as for example beams with fixed incidence angle ranges.

As a reference system for this analysis, we use the TerraSAR-X orbit and the according SAR parameters of the satellite and compute the coverage duration for AOIs within a length range between 40 and 200 km. In order to keep the results interpretable, the height remains constant. We therefore chose a constant AOI height of 40 km as a lower height simplifies the interpretation of the results. The outcome of the analysis is shown in **Figure 21** for the fastest (top) and the slowest coverage duration (bottom). The axes show the latitude and the AOI width while the color-bar represents the coverage duration. The according number of acquisitions for each AOI and acquisition direction are annotated in **Table 3**.

From **Figure 21** it can be seen that the slowest duration is symmetrical over latitude showing the typical pattern of single direction acquisitions. This makes sense since the numbers of acquisitions for single and mixed direction in **Table 3** are equal but for a mixed coverage more orbits can be used. Therefore, the coverage time from a single viewing direction is in general

Table 3: Number of required acquisitions for single and mixed acquisition direction for different AOI longitude dimensions.

AOI width [km]	$n_{acq,single}$	$n_{acq,mixed}$	
		Ascending	Descending
40	2	1	1
60	3	2	1
80	4	2	2
100	5	3	2
120	5	3	2
140	6	3	3
160	7	4	3
180	8	4	4
200	9	5	4

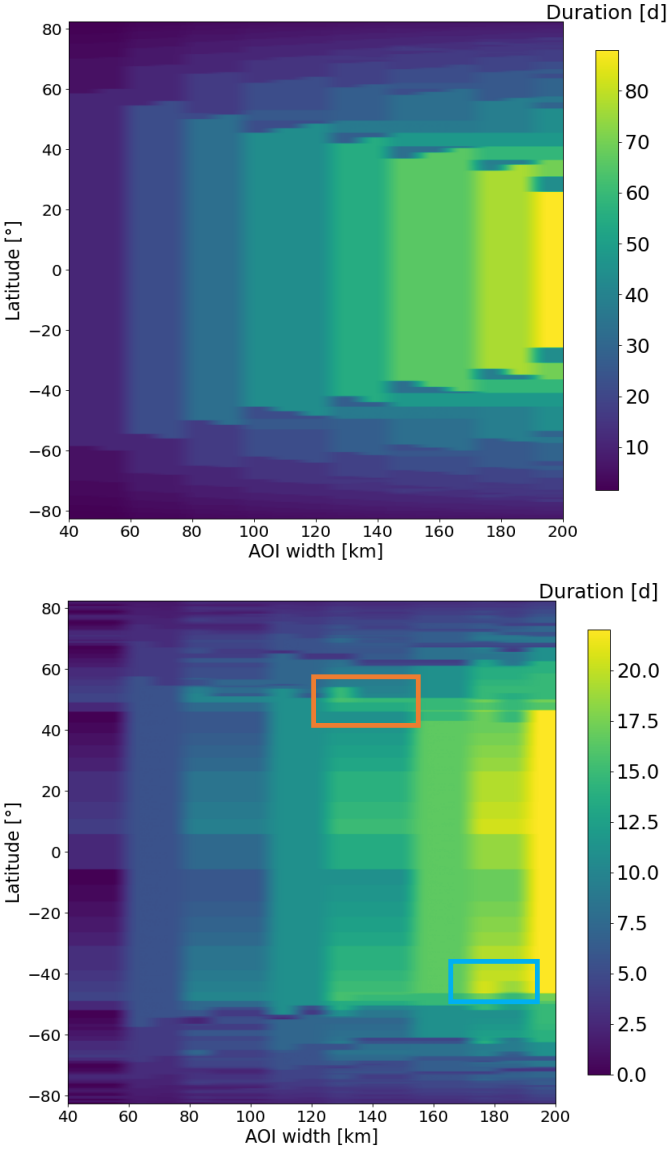

Figure 21: Slowest (top) and fastest (bottom) coverage durations for AOIs with l_{AOI} = [40, 200] km and h_{AOI} = 40 km over all latitudes. The orange rectangle (bottom) indicates a faster access from $n_o^{'}$ than from n_o. The blue rectangle (bottom) highlights a faster coverage for a slightly larger AOI.

higher than from a combined viewing direction.

In contrast to that, the fastest achievable coverage duration shows an asymmetrical behavior and fluctuates as well in latitude as also over the AOI length. One reason for that is the descending ground-track pattern and its variation over latitude as already described in section IV.A.b) (see **Figure 19**).

Another reason that superimposes with the descending ground-track pattern in latitude, is the distribution of acquisitions between orbits with an access to the AOI as described in section III.D. If the majority of the acquisitions have to be performed from one central orbit it can happen that the coverage from the minimum number of orbits with AOI access is faster than from a maximum number of orbits. As an example, such a case is highlighted in the orange rectangle in **Figure 21** (bottom).

Overall the results show that the longest duration obviously is obtained at the equator since the overlap at this latitude is the smallest. Furthermore, larger AOIs require more acquisitions than smaller ones but at the same time they can be accessed from additional adjacent orbits at lower latitudes. Thus, it can happen that larger AOIs require less time to be covered at certain latitudes than slightly smaller AOIs. For example, this can be seen in the blue rectangle in **Figure 21** (bottom) at a latitude of 45° and AOI length of 170 and 180 km.

C. Comparison to TerraSAR-X Acquisition Planning and Coverage Results from Commercial Software

For the validation of the presented methodology, we compare the estimation outcome to the according planning results from the TerraSAR-X mission (TSM) and also to a coverage analysis performed by means of the STK software. This comparison is first carried out for a Stripmap acquisition of an AOI with l_{AOI} = 100 km and h_{AOI} = 40 km. The TSM as well as the STK results are generated by analyzing the footprint of the ascending and descending Stripmap beams and their intersection with the AOI at the specified location. Additionally, the validation is conducted for a variety of differently sized AOIs in various locations. For the effective swath width with r_{swath} = 24 km as well as for the orbit characteristics, the parameters from the TSM are used with an orbit altitude of 514 km, an orbital inclination of 97.44°, a repeat cycle of 11 days and a total of 167 revolutions within one repeat cycle. As an example, the scenario is illustrated for a single (top) and a mixed (middle) acquisition direction TSM coverage and an ascending STK coverage (bottom) of the AOI from a right-looking direction in **Figure 22**. The illustration is showing the Stripmap beams (according to the TerraSAR-X full performance range [32]), the ARs and the ground-tracks of a Stripmap coverage at a latitude of Λ = 48.3° in the region of Bavaria. The results of the analysis of various AOIs are presented at the end of this section in **Table 5**.

From the illustration it can be seen that four Stripmap beams are required in both acquisition direction cases. In the TSM single acquisition direction case these are either beams seven to ten (indicated by the yellow colored beam number in **Figure 22** (top)), for an ascending coverage, or beams five to eight, for a descending TSM coverage. For the combined acquisition direction, the coverage begins on the western end of the AOI

Table 4: Comparison between estimation, TSM planning results (full performance range) and a coverage analysis with STK for an AOI with dimensions l_{AOI} = 100 km and h_{AOI} = 40 km.

	Estimation	TSM	STK
$n_{acq,single}$	4	4	4
$n_{acq,mixed}$	4 (2 asc., 2 desc.)	4 (2 asc., 2 desc.)	4 (2 asc., 2 desc.)
n_o	2	2	2
n_o'	1	1	1
$t_{cov,single}$	16.5 - 33 d	17 d	17 d
$t_{cov,mixed}$	7.5 – 16 d	11 d	11 d

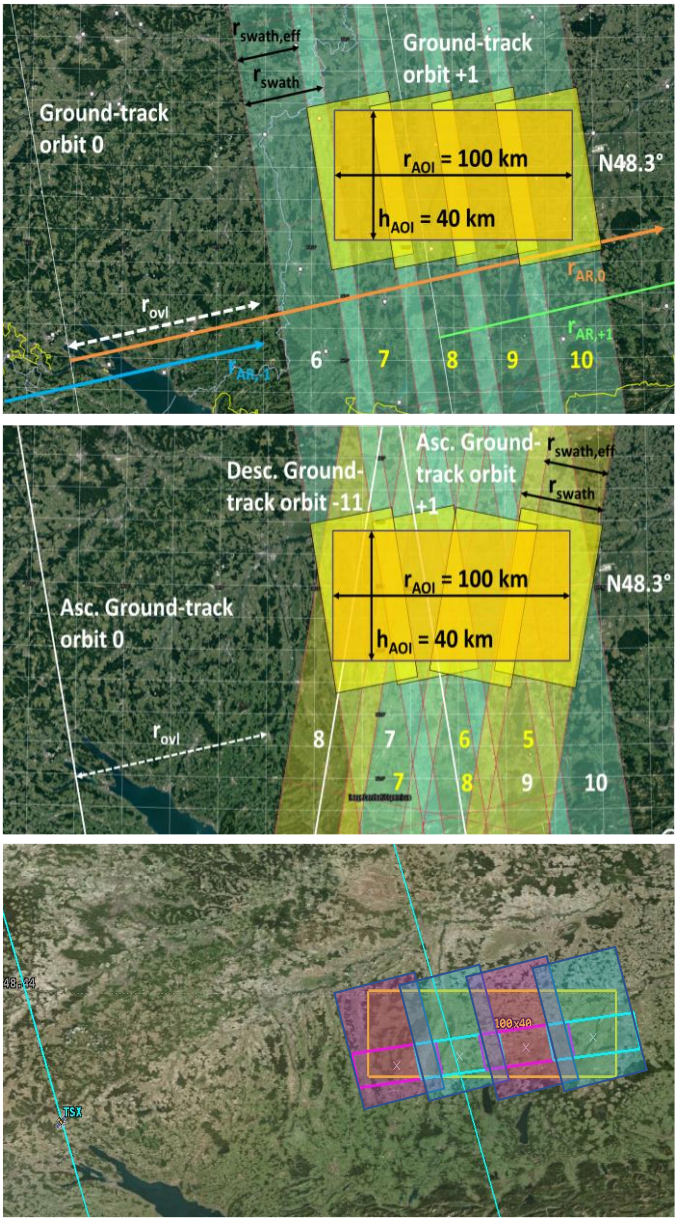

Figure 22: TerraSAR-X coverage from ascending-only (top) and ascending/descending combined direction (middle) of an AOI with l_{AOI} = 100 km and h_{AOI} = 40 km at latitude of Λ = 48.3°, visualized on GoogleEarth. The coverage of an identical AOI is also performed with the STK software, visible for an ascending coverage (bottom).

Table 5: Comparison between estimation and TerraSAR-X (TSX) mission planning results for various AOI dimensions

AOI parameters (r_{AOI}, h_{AOI}, Λ)	TSX estimation [d] Direction		TSX mission [d]	
	Single	Mixed	Single	Mixed
40 km, 40 km, 10°	5.5 – 22	4 – 11	11	4
40 km, 40 km, 61°	7.3 – 16.5	3.7 – 7.5	11	6
40 km, 40 km, 69°	7.3 – 16.5	2.8 – 6.3	11	6
60 km, 60 km, 20°	16.5 - 44	8.5 - 22	22	15
60 km, 60 km, 58°	14.7 – 25.7	5.3- 11	17	6
60 km, 60 km, 75°	8.8 – 15.4	4.4 – 6	11	6
100 km, 100 km, 3°	22 - 55	13.5 - 33	55	32
100 km, 100 km, 57°	18.3 – 33	14.7 - 19.5	22	16
100 km, 100 km, 67°	14 – 25.7	11 – 14.7	22	11
200 km, 200 km, 12°	44 – 99	22.5 – 55	93	44
200 km, 200 km, 55°	40.3 - 58	22 – 25.3	49	23
200 km, 200 km, 72°	26.4 - 28.6	14.2 – 15.8	27	16
500 km, 500 km, 0°	102.7 - 105	79.5- 104	105	99
500 km, 500 km, 50°	66 – 70.4	43 – 49.6	67	49
500 km, 500 km, 75°	32 - 37.8	15.6 - 20	32	20

with the ascending beams seven and eight and finishes on the eastern side with the descending beams five and six (indicated by the yellow colored beam number in **Figure 22** (middle)). Of course, it is also possible to start with descending beams on the western end and terminate the coverage with ascending beams. The detailed results of the comparison, including the STK analysis, are listed in **Table 4**. For the STK analysis, a more detailed presentation of the results can be found in the appendix in **Table 6**.

According to the definitions in (27) and (28) the estimation results for the coverage duration are given between the respective min/max values. From the comparison it can be seen that the acquisition planning outcome as well as the STK coverage analysis fit well into the range of the estimated duration for both single and mixed acquisition directions. The difference of 0.5 d between both the TSM/STK coverage and the coverage estimation, results from the averaging of the coverage duration for different AOI locations in (28).

The parameters of the TSM and the STK coverage appear to be optimal for a fast coverage in this latitude which is accurately represented by the approximation. Additionally, the slowest coverage estimation of 33 d is obtained from only one orbit (n = 0) with four required acquisitions. Applying only one orbit to the TSM or the STK coverage then also results to a duration of 33 d. The outcome of the estimation and the acquisition planning or the STK data in this case is identical.

Looking at the results for various AOIs between 40 and 500 km as well in length as in height in **Table 5**, one can see that nearly all planning results are correctly approximated. For almost all of the analyzed scenarios the TSM coverage duration is within the range of the estimated coverage duration. In one scenario (200 km x 200 km at 72°) the planned coverage duration slightly exceeds the maximum estimated coverage duration by a total average of 0.2 days. The reason for this deviation is the averaging of the results according to equation (28) occasionally resulting in slighter higher or lower durations than estimated.
Furthermore, no deviations occur due to the assumption that the beams from adjacent orbits maintain a constant angular relation over latitude. As explained in section III.E, the ground-tracks of the orbits reduce their distance with increasing latitude which also changes the alignments of the beams between the adjacent orbits. As a consequence, gaps appear between the beams of adjacent orbits and the actual coverage thus requires more beams for the full AOI coverage than estimated. Therefore, general margins were introduced in order to adjust the number of required acquisitions (see **Table 2**). **Table 4** and **Table 5** show that for all cases except one, these margins are sufficient to correctly determine the number of required acquisitions and ultimately to correctly estimate the coverage duration.
In conclusion the approach has proven to work as intended since all planning as well as the STK results are correctly estimated. However, if a more detailed coverage information is needed e.g. for a precise operational planning, the planning tools and in particular the STK software analysis are to be preferred. They provide very comprehensive and precise results such as the exact duration in milliseconds for each beam that accesses the AOI or the coverage percentage for each pass with AOI access just to mention a few.

V. Summary

In this paper we presented a dedicated approach to estimate the coverage duration for any rectangular AOI at a given latitude and a specified SAR configuration. In order to give an overview of the processing steps that are involved in the determination of the coverage duration, in the following we summarize the individual sections of this paper. The complete algorithm to estimate the coverage duration is therefore shown as a block diagram in **Figure 23**.
At first the input parameters in terms of the orbit characteristics (i, R, D), the AOI characteristics (l_{AOI}, h_{AOI}, Λ), the system's effective swath width r_{swath} and if beams with fixed or continuously steerable incidence angle ranges apply, are defined (**Figure 23** A).
These are then used on the one hand to determine the number of acquisitions that are required for a full coverage of the AOI (**Figure 23** B1). Based on the acquisition direction scenario (single or mixed direction) the effective coverage variates and different height limit definitions apply. Therefore, the number of required acquisitions depends on the single or combined use of ascending and descending acquisitions and is labeled accordingly.
On the other hand, the input parameters are also utilized to determine the accessibility of the AOI which is expressed by means of the maximum and minimum number of orbits n_o/n_o' that provide an access opportunity to the AOI (**Figure 23** B2). In order to evaluate if a coverage from n_o is applicable or

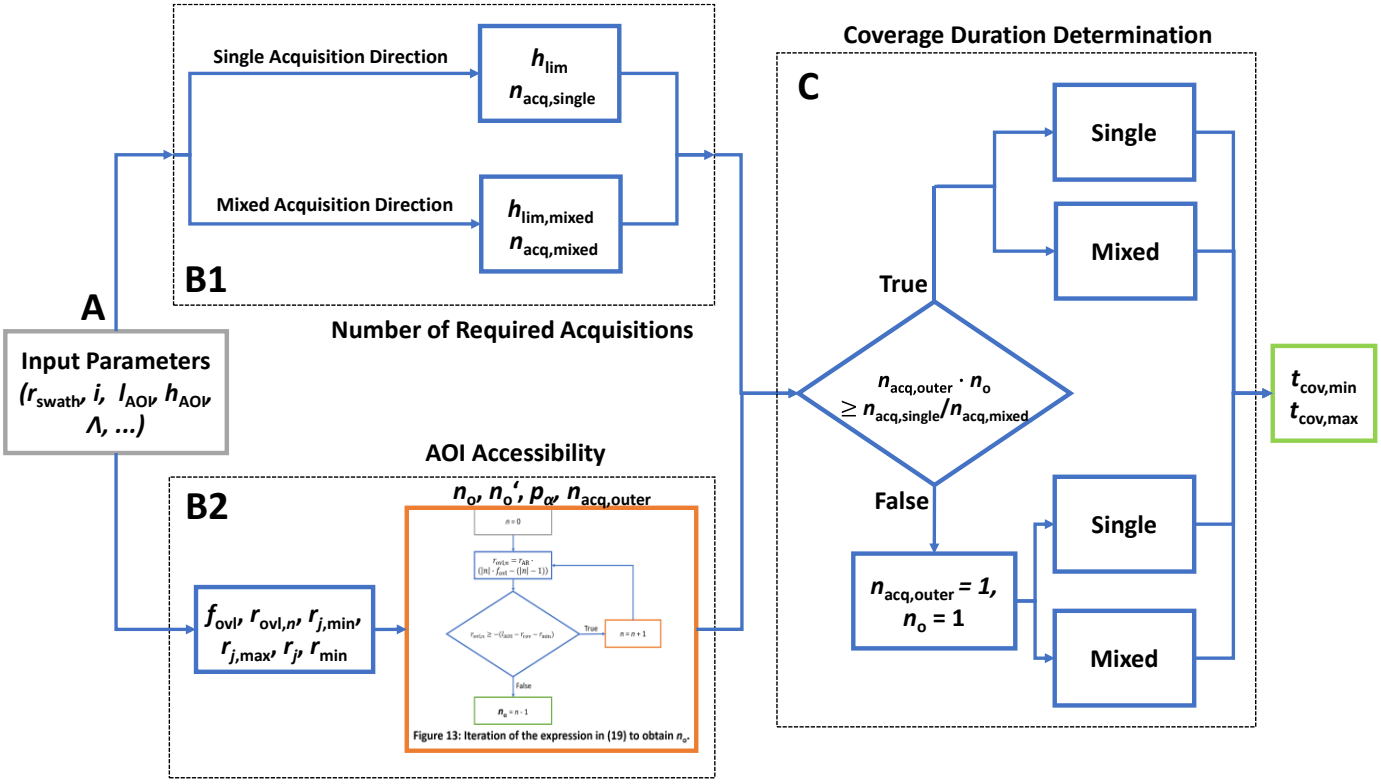

Figure 23: Block diagram illustrating the determination of the minimum and maximum achievable coverage duration based on the definition of the orbit, the AOI, the latitude, the swath width and restrictions such as the use of only single acquisitions direction. The illustration in the orange block in B2 refers to Figure 13.

unlikely, the proportion for an AOI to be located in this range p_α is also determined in the same step.

Additionally, the distribution of the acquisitions between the orbits in n_o is determined in the same step according to (23). This is used in the following process to determine if the number of required acquisitions can be shared equally between the orbits with an access or if the adjacent orbits only cover a fraction of the AOI.

In the first case the ground-track pattern is generated directly for the use of either single or mixed direction acquisitions. By combining the resulting pattern with the respective maximum and minimum number of orbits with AOI access as well as the respective number of acquisitions, the coverage duration t_{cov} for equally distributed acquisitions is eventually obtained according to (27) and (28) (**Figure 23** C).

In the latter case the majority of acquisitions have to be performed from the central orbit. The number of acquisitions from the central orbit are then determined before generating the ground-track pattern. As these acquisitions dominate the coverage duration, the acquisitions from the adjacent orbits are neglected in the further process. As a result, the number of required acquisitions is set to the number of acquisitions from the central orbit and n_o is set to one. Combining these new parameters with the ground-track pattern for single and mixed direction then yields the coverage duration for the imbalanced acquisition distribution (**Figure 23** C).

The coverage time as the final result is given in a range representing the fastest and the slowest achievable coverage duration for each AOI. In order to provide a full evaluation of a system's coverage duration performance the process is repeated for multiple AOIs with different dimensions and over the entire possible latitude range as shown in **Figure 21**.

VI. Conclusion

Commonly the coverage performance of a SAR system is evaluated using extensive simulation configurations to find the intersections between the system's footprint and the AOI grid-points of multiple different AOIs. However, the paper has demonstrated that by introducing a simplified approach that explicitly approximates the coverage duration based on a geometric analysis, the complexity is significantly reduced. As a result, the comparison of the coverage duration analysis between various AOI sizes as well as between different system or orbit configurations, can be performed quick and with considerably less effort.

In this context, the geometric features for an AOI coverage are analysed and the required coverage parameters are defined. It is shown how the number of acquisitions required to cover an AOI as well as the accessibility to an AOI are determined and how the coverage duration is approximated by combining these outcomes with the respective ground-track pattern.

The according simulation results are presented for the purpose of providing a representative overview of a system's coverage capability. Therefore, the results are presented in a range of different AOI dimensions. This also includes adapting the full latitude spectrum that can be realized for the according orbit as well as considering the use of single and mixed acquisition directions.

In order to validate the methodology, the outcome is compared with actual planning data from the TerraSAR-X mission. The presented results show that for the majority of cases the planned coverage duration is well approximated. The TSM coverage duration then lies within the range of the minimum and maximum computed coverage duration. In contrary to the assumption that the beams of adjacent orbits remain parallel from the equator to the poles, the angle between the beams of adjacent orbits increases with increasing absolute latitude. As a consequence, some of the planned coverages require actually more acquisitions to completely cover an AOI and thus the according coverage duration is longer than estimated. A solution to overcome this deviation was introduced by adding a margin to the number of required acquisitions. This margin works well and successfully supports the correct coverage duration estimation.

However, for future work the methodology can be improved by including the angular separation of the adjacent beams in the computation of the required number of acquisitions. Despite the increase in complexity and a more detailed knowledge of the satellite's orbit parameters, the results then become more accurate and adding the respective margins can be discarded.

Overall the approximation method generates accurate results which provide a well-structured overview of the coverage duration performance of a given SAR system. Furthermore, the input is based on only few basic parameters which can be manipulated straightforwardly. This makes it practicable to evaluate different configurations and compare different systems.

References

[1] J. J. Morrison, "A System of Sixteen Synchronous Satellites for World-wide Navigation and Surveillance", *Technical Dept. of Transportation Federal Aviation Administration Systems Research and Development Service, FAA RD-73-30*, pp. 1–52, Mar. 1973.

[2] Z. Song, G. Dai, M. Wang, X. Chen, "A Novel Grid Point Approach for Efficiently Solving the Constellation-to-Ground Regional Coverage Problem", *IEEE Access*, vol. 6, Aug. 2018.

[3] J. Sipps, L. Magruder, "Envelope-Based Grid-Point Approach: Efficient Runtime Complexity for Remote Sensing Coverage Analysis", *Journal of Spacecraft and Rockets*, vol. 60 (4), Apr. 2023.

[4] H. Li, D. Li, "A multi-index assessment method for evaluating coverage effectiveness of remote sensing satellite", *Chinese Journal of Aeronautics*, vol. 31 (10), pp. 2023 – 2033, Jun. 2018.

[5] C. Han, X. J. Gao, X. G. Sun, "Rapid satellite-to-site visibility determination based on self-adaptive interpolation technique", *Science China Technological Science*, vol. 60, pp. 264 – 270, Dec. 2016.

[6] Satellite Tool Kit: http://www.agi.com/products/by-producttype/applications/stk/, last visited 12-15-2023.

[7] FreeFlyer Astrodynamics Software: https://ai-solutions.com/freeflyer-astrodynamic-software/, last visited 12-15-2023.

[8] Y. Ulybyshev, "General Analysis Method for Discontinuous Coverage Satellite Constellations", *Journal of Guidance, Control and Dynamics*, vol. 38 (12), Aug. 2015.

[9] C. Han, Y. Zhang, S. Bai, "Geometric Analysis of Ground-Target Coverage from a Satellite by Field-Mapping Method", *Journal of Guidance, Control and Dynamics*, vol. 44 (8), Aug. 2021.

[10] H. Wang, S. Bai, "A versatile method for target area coverage analysis with arbitrary satellite attitude maneuver paths", *Acta Astronautica*, vol. 194, pp. 242 – 254, May 2022.

[11] X. He, H. Li, "General analysis method for global revisit characteristics of satellite constellation with repeating ground tracks", *Acta Astronautica*, vol. 202, pp. 319 – 332, Jan. 2023.

[12] Y. Ulybyshev, "Satellite Constellation Design for Complex Coverage", *Journal of Spacecraft and Rockets*, vol. 45 (4), pp. 843 – 849, Aug. 2008.
[13] F. Bunkheila, E. Ortore, C. Circi, "A new algorithm for agile satellite-based acquisition operations", *Acta Astronautica*, vol. 123, pp. 121 – 128, Jun. 2016.
[14] S. M. Henn, J. A. Fraire, H. Hermanns, "Polygon-Based Algorithms for N -Satellite Constellations Coverage Computing", *IEEE Transactions on Aerospace and Electronic Systems*, vol. 59 (5), pp. 7166-7182, Jun. 2023
[15] J. Middour, "An efficient technique for computation of satellite earth coverage", *Aerospace Sciences Meeting (AIAA)*, vo. 27, Jan. 1989
[16] D. R. Brooks, "An introduction to orbit dynamics and its application to satellite-based earth monitoring systems", *NASA Reference Publication (RP)*, Nov. 1977.
[17] R. Boain, "A-B-Cs of sun-synchronous orbit mission design", *AAS/AIAA Space Flight Mechanics Meeting*, vol. 14, Feb. 2004.
[18] X. Luo, M. Wang, G. Dai, Z. Song, „Constellation Design for Earth Observation based on the Characteristics of the Satellite Ground Track", *Advances in Space Research*, vol. 59, pp. 1740 – 1750, Jan. 2017.
[19] M. Younis, P. López-Dekker, F. Bordoni, P. Laskowski, G. Krieger, „Exploring the trade-space of MIMO SAR", *2013 IEEE International Geoscience and Remote Sensing Symposium (IGARSS)*, Jul. 2013.
[20] A. Bojarski, M. Bachmann, J. Böer, T. Kraus, C. Wecklich, U. Steinbrecher, N. Tous Ramon, K. Schmidt, P. Klenk, C. Grigorov, M. Schwerdt, M. Zink, "TanDEM-X Long-Term System Performance After 10 Years of Operation", *IEEE Journal of Selected Topics in Applied Earth Observations and Remote Sensing*, vol. 14, pp. 2522-2534 Jan. 2021.
[21] A. Bojarski, M. Bachmann, "A Simplified Method to Approximate the AOI Coverage Duration in Single Acquisition Direction for SAR Satellites with Repeat Ground Track Orbits", *15th European Conference on Synthetic Aperture Radar (EUSAR)*, May, 2024.
[22] P. H. Laskowski, "The Traditional and Modern Look at Tissot's Indicatrix", *The American Cartographer*, vol. 16 (2), pp. 123 – 133., 1989.
[23] J. Mittermayer, S. Wollstadt, P. Prats-Iraola, R. Scheiber, "The TerraSAR-X Staring Spotlight Mode Concept", *IEEE Transactions on Geoscience and Remote Sensing*, vol. 50 (6), Jun. 2014.
[24] Y. Xiang, N. Jiao, R. Liu, F. Weng, H. You, X. Qiu, K. Fu, "A Geometry-Aware Registration Algorithm for Multiview High-Resolution SAR Images", *IEEE Transactions on Geoscience and Remote Sensing*, vol. 60, Sep. 2022.
[25] Th. Toutin, "Opposite side ERS-1 SAR stereo mapping over rolling topography", *IEEE Transactions on Geoscience and Remote Sensing*, Vol. 34 (2), pp. 543 - 549, Mar. 1996.
[26] P. Rizzoli, B. Bräutigam, M. Zink, "TanDEM-X Large-Scale Study of Tropical Rainforests for Spaceborne SAR Calibration in X-band", *IEEE Transactions on Geoscience and Remote Sensing*, vol. 60, Sep. 2022.
[27] B. Bauer-Marschallinger et. al, "The normalised Sentinel-1 Global Backscatter Model, mapping Earth's land surface with C-band microwaves", *Scientific Data*, vol. 8, Oct. 2021.
[28] Y. Yang, C. Hwang, W. Hung, T. Fuhrmann, Y. Chen, S. Wei, "Surface Deformation from Sentinel-1A InSAR: Relation to Seasonal Groundwater Extraction and Rainfall in Central Taiwan", *Remote Sensing*, vol. 11 (23), Nov. 2019.
[29] S. Buckreuss, R. Werninghaus, W. Pitz, "The German Satellite Mission TerraSAR-X", *IEEE Radar Conference*, May 2008.
[30] B. Bräutigam, M. Schwerdt, M. Bachmann, "An Efficient Method for Performance Monitoring of Active Phased Array Antennas", *IEEE Transactions on Geoscience and Remote Sensing*, vol. 47 (4), pp. 1236 – 1243, Apr. 2009.
[31] M. Bachmann, M. Schwerdt, B. Bräutigam, "Accurate Antenna Pattern Modeling for Phased Array Antennas in SAR Applications—Demonstration on TerraSAR-X", *Active Antennas for Space Applications*, vol. 2009, Jun. 2009.
[32] T. Fritz et al., "TerraSAR-X Basic Product Specification Document", DLR, public version 1.9, Oct. 2013.
[33] O. Alvarez-Salazar, S. Hatch, J. Rocca, P. Rosen, S. Schaffer, Y. Shen, "Mission design for NISAR repeat-pass interferometric SAR", *Proc. SPIE 9241, Sensors, Systems, and Next-Generation Satellites*, vol. 8, Nov. 2014.
[34] E. Ortore, M. Cinelli, C. Circi, "A ground track-based approach to design satellite constellations", *Aerospace Science and Technology*, vol. 69, pp. 458 – 464, Oct. 2017.
[35] C. Circi, E. Ortore, F. Bunkheila, „Satellite constellations in sliding ground track orbits", *Aerospace Science and Technology*, vol. 39, pp. 395 – 402, May 2014.
[36] G. Krieger, A. Moreira, H. Fiedler, I. Hajnsek, M. Werner, M. Younis, M. Zink, "TanDEM-X: A Satellite Formation for High-Resolution SAR Interferometry", *IEEE Transactions on Geoscience and Remote Sensing*, vol. 45 (11), pp. 3317 – 3341, Nov. 2007.
[37] X. Luo, M. Wang, G. Dia, X. Chen, "A Novel Technique to Compute the Revisit Time of Satellites and Its Application in Remote Sensing Satellite Optimization Design", *International Journal of Aerospace Engineering*, vol. 2017, No. 6, Jan. 2017.
[38] E. Ortore, C. Circi, F. Bunkheila, C. Ulivieri, "Earth and Mars observation using periodic orbits", *Advances in Space Research*, vol. 49, pp. 185 – 195, Jan. 2012.
[39] R. Hopkins, "Long-Term Revisit Coverage Using Multi-Satellite Constellations", *AIAA Astrodynamics Conference*, Aug. 1988.
[40] J.C. King, "Quantization and symmetry in periodic coverage patterns with applications to earth observation", *AAS/AIAA Astrodynamics Specialist Conference*, Dec. 1975.

APPENDIX

Table 6: Exact results from the STK analysis according to the scenario descried in Figure 22 including the acquisition direction, the timestamp and the duration of the access to the AOI during the pass for each used beam.

Single direction coverage		
# acquisition	timestamp	AOI Access duration
1 (asc)	17-08-2024-16:52:59.460	8.313 s
2 (asc)	23-08-2024 16:44:26.631	8.649 s
3 (asc)	28-08-2024 16:53:00.166	8.646 s
4 (asc)	03-09-2024 16:44:24.250	8.392 s
Mixed direction coverage		
# acquisition	timestamp	AOI Access duration
1 (asc)	17-08-2024 16:52:59.460	8.323 s
2 (desc)	19-08-2024 05:36:26.636	8.377 s
3 (desc)	24-08-2024 05:45:01.933	8.656 s
4 (asc)	28-08-2024 16:52:59.799	8.664 s

AUTHOR BIOGRAPHIES

Allan Bojarski received the Dipl. -Ing. degree in aerospace engineering from the Technical University of Munich (TUM), Munich, Germany, in 2014.
After 2 years performing battery simulations for the Daimler R&D department in Ulm, Germany, in 2016 he joined the Microwaves and Radar Institute at the German Aerospace Center (DLR) in Oberpfaffenhofen, Germany. He is currently involved in various spaceborne SAR projects as a mission engineer. In this context, he is responsible for the long-term system monitoring of the TerraSAR-X/TanDEM-X satellites and the scientific acquisition planning for the TanDEM-X mission. Furthermore, he is designing mission scenarios, SAR satellite formations and observation concepts for several SAR missions such as Tandem-L or HRWS.

Markus Bachmann received the Dipl.-Ing. degree from the Technical University of Karlsruhe, Germany, in 2005 and the PhD degree in electrical engineering from the Karlsruhe Institute of Technology, Germany, in 2015. In 2005, he joined the Microwaves and Radar Institute, German Aerospace Center. From 2005 to 2011, he was in charge of the calibration of the TerraSAR-X/TanDEM-X antenna model. From 2008 to 2012, he was responsible for the planning and execution of the TanDEM-X commissioning phase and was in charge of the interferometric calibration and global monitoring of the TanDEM-X mission. He was ground segment project manager of the Tandem-L/Rose-L-Tandem project between 2016 and 2023.

Since 2012, he leads the “mission engineering” group, which is responsible for the TanDEM-X instrument, instrument operations, system performance monitoring and acquisition planning. The group furthermore develops future SAR mission concepts and advanced observation strategies and was or is involved in future mission proposals like Tandem-L, Rose-L Tandem, HRWS, and TerraSAR-FOX.